Faculty of Science

CHARACTERIZATION OF UV RESISTANT MOLECULES IN TREMBLING ASPEN TREE (*POPULUS TREMULOIDES MICHX.*) POWDER

2023 | ABU HARERA NADEEM

B.Sc. HONOURS THESIS – CHEMICAL BIOLOGY

THOMPSON RIVERS UNIVERSITY

CHARACTERIZATION OF UV RESISTANT MOLECULES IN TREMBLING ASPEN TREE (*POPULUS TREMULOIDES MICHX.*) POWDER

by

ABU HARERA NADEEM

A THESIS SUBMITTED IN PARTIAL FULFILLMENT

OF THE REQUIREMENTS FOR THE DEGREE OF

BACHELOR OF SCIENCE (HONS.)

in the

DEPARTMENTS OF BIOLOGICAL SCIENCES

AND PHYSICAL SCIENCES

(Chemical Biology)

This thesis has been accepted as conforming to the required standards by:

Natasha Ramroop Singh (Ph.D.), Thesis Supervisor, Dept. Biological Sciences

Kingsley Donkor (Ph.D.), Co-supervisor, Dept. Physical Sciences

Lyn Baldwin (Ph.D.), External examiner, Dept. Biological Sciences

Dated this 25th day of April, 2023, in Kamloops, British Columbia, Canada

ABSTRACT

Commercial sunscreen products offer protection against ultraviolet (UV) radiation. This type of radiation can cause numerous health effects on all organisms, such as premature aging, cancer, and decreased immunity against infections. Hence, it is important for organisms to apply compounds with UV resistant properties, such as sunscreen, before engaging in activities outside in the Sun. However, the chemical compositions of commercial sunscreens can cause serious environmental harm. When sunscreen is washed from skin, toxic chemicals can enter waterways and, for example, can diminish growth of aquatic life. As a solution to this problem, naturally derived sunscreen can be used, which can be found on the barks of trees such as the Trembling Aspen tree (*Populus tremuloides*) in the form of a grey/white powder. Based on this, there potentially are UV resistant molecules in the powder from *Populus tremuloides* that have not yet been elucidated based on literature searches. It was found that there are approximately five molecules in the powder that absorb UV light and this work has partially characterized some of these using, CE (Capillary Electrophoresis) IR (Infrared Spectroscopy), and ^{1}H-NMR (Nuclear Magnetic Resonance). These molecules may have alkenes, alkynes, amines, amides, and aldehydes, which have the potential to absorb UV radiation—making them UV resistant.

Thesis Supervisor: Natasha Ramroop Singh (Assistant Teaching Professor).

ACKNOWLEDGEMENTS

I would like to thank Dr. Natasha Ramroop Singh, Dr. Kingsley Donkor, Dr. Lyn Baldwin, Dr. Louis Gosselin, and the Department of Biology and Chemistry at TRU for their support and guidance throughout the project. I appreciate the Canada Foundation for Innovation (CFI) for providing the necessary analytical and spectroscopic instrumentation. I also would like to thank Isaac Stephens, Michelle Boham, Dr. Dipesh Prema, Dr. Bruno Cinel, and Dr. Don Nelson for their support. Finally, I wish to acknowledge the TRU Internal Research Fund, for providing the funding for the consumables in this project.

TABLE OF CONTENTS

LIST OF FIGURES

LIST OF TABLES

INTRODUCTION

Trembling Aspen Tree (*Populus tremuloides* Michx.)

The Trembling Aspen species is deciduous, perennial, can grow up to 25 metres tall, has the broadest distributional range of all tree species in North America, and is one of the most genetically diverse plant species known (Lindroth & St. Clair, 2013; Mitton & Grant, 1996; Government of British Columbia, n.d.; Evert & Eichhorn, 2013). Specifically, the Trembling Aspen tree grows in Alaska, Canada, and to the South of Mexico (The National Wildlife Federation, n.d.). In addition, the Trembling Aspen species is abundant in North America and controls biodiversity by helping to maintain habitats in forests, making them a foundational species (Endress et al., 2012; Kashian et al., 2007; Zegler et al., 2012; Ellison et al., 2005).

The life cycle of Trembling Aspen trees involves a form of reproduction that uses pollen and eggs that are in catkins (The National Wildlife Federation, n.d.). This form of reproduction relies on the wind to carry the pollen to the eggs in the catkins in order to fertilize them (The National Wildlife Federation, n.d.). Trembling Aspen trees can also reproduce asexually by shooting new stems from their single root system, creating a clone which is the culmination of all the stems and their root system (The National Wildlife Federation, n.d.).

Trembling Aspen is also well-known for its characteristically smooth, white bark that often has a white powder on its surface. Anecdotally, this powder is believed to act as a "sunscreen" for the tree, especially on the south-facing side of the tree. Like commercial sunscreens, the white powder may have the potential to absorb UV radiation and emit it back into the environment. However, commercial sunscreens contain chemicals such as oxybenzone that, when washed from skin, can enter waterways and reduce the growth of green algae—stressing the need for a less toxic sunscreen (Califf & Shinkai, 2019). The application of the white powder as a natural sunscreen is supported by Native and Indigenous people, as they have incorporated this white powder into their traditions and have used it for protection against UV radiation from the Sun (Plant Watch Nature Alberta, n.d.; University of Saskatchewan, 2021; Medieval Manor Gardens, n.d.).

Trembling Aspen Tree Bark and Powder

In most trees, photosynthesis occurs primarily in its leaves; however, Trembling Aspen has photosynthetic bark with has green chlorenchyma cells found beneath the bark's outer surface (The

National Wildlife Federation, n.d.; National Geographic Society, n.d.). Specifically, the bark has the pigments beta-carotene, pheophytin, chlorophyll-a, chlorophyll-b, and xanthophyll that are responsible for photosynthesis (University of Colorado Boulder, 2015, Figure 1). The preferred light for photosynthesis is within the blue and red ranges which are 425-450 nm and 600-700 nm, respectively (Vernier, 2018). But, since sunlight encompasses other types of light, some UV light is also absorbed during photosynthesis and can degrade the plant (Valenta et al., 2020).

As Trembling Aspen is a deciduous tree, it is believe that this photosynthetic bark extends the photosynthetic season of these trees (The National Wildlife Federation, n.d.).

However, this bark is thin and can be easier for UV radiation to penetrate the layers of the bark such as the periderm or perhaps the living phloem and cause degradation (University of Minnesota, n.d.; United States Department of Agriculture, n.d.). Due to this, Trembling Aspen may expend energy and effort to make the white powder in order to protect itself from UV degradation.

Figure 1. Photo of Trembling Aspen's photosynthetic bark taken at Lac du Bois in Kamloops, BC, Canada.

The powder found on Trembling Aspen's bark has been described as mature bark cells that are shed from the tree allowing light to penetrate the cork and cambium, eventually reaching the chlorenchyma (University of Colorado Boulder, 2015). Reports also indicate the powder initial

colour is orange and composed of conglutinated cells that become white with age (University of Colorado Boulder, 2015). On the other hand, the powder may primarily be composed of naturally occurring yeast or lichens (The Survival University, n.d.), or made of anti-microbial compounds that help to fight off bacteria (St-Pierre et al., 2018).

There are many mechanisms for how the powder could be made in Trembling Aspen trees. The powder could simply be the accumulation of dead bark cells from the cambium. Or, the powder could be a secondary metabolite that the tree makes by expending energy. Plants and humans make a diverse number of secondary metabolites (Torres & Schmidt, 2019; Teoh, 2015). The powder would be classified as a secondary metabolite instead of a primary metabolite because primary metabolites are similar in each species, while secondary metabolites are different in every species and the powder is unique to Trembling Aspen (Byjus, n.d.). Plants make secondary metabolites, such as phenolics and terpenes, to defend themselves against environmental constraints and to be competitive within their environment (Guerriero et al., 2018; Teoh, 2015; Pang et al., 2021).

If considering that the purpose of the powder is to protect Trembling Aspen's photosynthetic bark from too much exposure to UV radiation, then it would seem logical for the plant to make the secondary metabolite as it protects the tree from environmental damage. Vascular rays and the formation of heartwood are known to produce secondary metabolites in trees (Celedon & Bohlmann, 2017; Sandved et al., 1993). Some secondary metabolites are made by taking the carbon from the sugars that are produced during photosynthesis and metabolizing them to make other compounds, one of which is erythrose-4-phosphate (Sinha et al., 2019). This compound gets fed into the Shikimic acid pathway and makes aromatic amino acids that can make nitrogen-containing secondary products such as nicotine or polyamines, or phenolic compounds like flavonoids or simple phenolics (Sinha et al., 2019). However, the secondary metabolites made from vascular rays or heartwood formation tend to stay within the interior of the bark (Celedon & Bohlmann, 2017; Barlow, 2005). They perhaps could make their way to the outside of bark through accumulating in the dead cells that make up the outer layer of the bark.

Photooxidative Stress

Photooxidative stress occurs when the energy dissipation mechanisms and structures that are used for photosynthesis are not developed yet and, consequently, reactive oxygen species are

created since there is a buildup of energy in chloroplasts (Muñoz & Munné-Bosch, 2017). This type of stress happens in senescing leaves or during cold temperatures (Muñoz & Munné-Bosch, 2017). Since Trembling Aspen is deciduous and sheds its leaves during the winter, the energetically expensive chemicals that make up the chlorophyll in the leaves are potentially degraded and lost, so the photosynthetic bark may act to offset the deciduous habit.

Existing Chemicals in Trembling Aspen Bark and Powder

Previous researchers have identified anti-microbial compounds in the powder as flavonoid structures (St-Pierre et al., 2018). In plants, flavonoids are located in vacuoles of cortical cells and are made through the phenylpropanoid pathway that forms 4-coumaroyl-CoA from phenylalanine which then enters the flavonoid pathway (Hassan & Mathesius, 2012; Falcone Ferreyra et al., 2012). Interestingly, flavonoids have structures that absorb UV radiation such as double bonds, so, the powder could be gaining UV resistance from antimicrobial compounds.

In addition, salicin—which is a glucoside—has also been isolated from Trembling Aspen, along with a compound termed 'populin' (Pearl & Darling, 1959). Salicin was found to be o-hydroxymethylphenyl-O-β-D-glucopyranoside, while synthetic populin was found to be 6-benzoylsalicin (Pearl & Darling, 1959). Another glucoside termed 'tremuloidin' was also isolated from the bark of Trembling Aspen and was found to be 2-benzoylsalicin, which is a monobenzoate of salicin and an isomer of populin (Pearl & Darling, 1959). The structure of salicin has an aromatic group along with hydroxyl functional groups, of which the former can absorb UV radiation, thus, it could be possible that this molecule or isomers of it are also responsible for UV resistance.

Other researchers investigating volatiles released from Trembling Aspen bark have identified 1-hexanol, benzyl alcohol, benzaldehyde, and nonanal (Borden et al., 1998). These volatiles disrupted the secondary attraction by mountain pine beetles where they kill living pines (*Dendroctonus ponderosae* Hopkins). The compound 1-hexanol was able to disrupt secondary attraction by itself, while the other 3 compounds had to be in binary, ternary, or quaternary combinations with each other to have a disruption effect (Borden et al., 1998). The structures of benzyl alcohol, benzaldehyde, and nonanal have double bonds or conjugated pi-bond electron systems which have the ability to absorb UV radiation, so, it is possible some of these compounds could be present in Trembling Aspen's powder.

UV Radiation and its Forms

With exposure to UV radiation being one of the leading causes of human skin cancer and other human skin diseases, it is important to apply sunscreen before being exposed to the sun (D'Orazio et al., 2013). UV radiation is light that has photons with high energy compared to visible light, and is a form of electromagnetic light (Rockett, 2019; U.S. Food and Drug Administration, 2020). There are three types of UV radiation: UVA, UVB, and UVC (U.S. Food and Drug Administration, 2020). The first form has long wavelengths allowing it to go beyond the Earth's ozone layer, something UVB and UVC radiation cannot do as they have shorter wavelengths (U.S. Food and Drug Administration, 2020). However, some UVB rays get through the ozone layer and can be absorbed by plants and reach the outer layer of human skin, or the epidermis (U.S. Food and Drug Administration, 2020). UVA rays go further and can reach the middle portion of the skin, which is the dermis (U.S. Food and Drug Administration, 2020). All forms of UV radiation can be emitted by the sun and not only damage skin, but also materials such as plastic.

Mechanism of UV Radiation

If UV radiation encounters skin or other materials, then, through the high-energy photons in UV radiation, it can break bonds that compose those materials (Rockett, 2019). By breaking bonds, the material becomes shorter and decreases molecular weight which results in degradation by lessening strength, ductility, colour, and texture. As for skin, UV radiation causes kinks in thymine bonds that are present in deoxyribonucleic acid, or DNA. This can lead to mutations or skin cancer. Hence, why sunscreen is important to use.

Properties of UV Resistant Molecules and Mechanism

To overcome the deleterious effects of UV radiation, certain molecules with UV resistant properties are used. UV resistance is commonly displayed in sunscreens as they consist of chemicals that can protect human skin. Molecules that have this property may contain double bonds aromatic rings, highly electronegative atoms, or metals. For instance, oxybenzone is a common molecule that is present in most sunscreens whose structure consists of aromatic groups

(D'Orazio et al., 2013). A common structural pattern in most UV resistance molecules in sunscreens is the presence of double bonds. These bonds absorb UV radiation and emit it back to the environment which protects the material or skin it is coated on as the UV radiation does not get past the molecule. Metals act in a similar way since they have a lattice structure and share a cloud of delocalized electrons that interfere with UV light by reflecting it back to the environment (Omnexus, n.d.; Rockett, 2019; Steeley et al., 2014).

Characterization Techniques

When dealing with unknown molecules, characterization techniques are used to ascertain the chemical structures and functional groups (Impact Analytical, 2022). Knowing the structure is the first step to identifying the molecule's functionality and applicability as a natural sunscreen. To do this, information from techniques such as Fourier Transform Infrared spectroscopy (FTIR), Capillary Electrophoresis (CE), and Nuclear Magnetic Resonance spectroscopy (NMR) was gathered. With this information, deriving the structure of the unknown molecules was similar to solving a puzzle, with each piece of information validating the placement of a functional group or a carbon atom.

Fourier Transform Infrared Spectroscopy (FTIR)

In the IR region, there are three subregions which are the near, mid, and far infrared regions. The near IR region is between 14000-4000 cm^{-1}, while the mid and far IR regions are from 4000-400 cm^{-1} and 400-10 cm^{-1}, respectively (Systems Chemistry, n.d.). FTIR detects frequencies in these regions that are absorbed by the bonds or groups within molecules (Mathias, 2015). Absorption in this case refers to the frequency of the absorbed radiation matching the vibrational frequency of the bond or functional group (Systems Chemistry, n.d.). Typically, when a spectrum is recorded, the transmittance is observed on the y-axis—not the absorbance. Transmittance is the percentage of energy that passes through a molecule or bond that is not absorbed (Sigma Aldrich, n.d.). On the x-axis, wavenumber is recorded, which is the number of wavelengths in a certain distance. Each bond type vibrates at a specific frequency, hence, FTIR analysis is useful for determining specific functional groups. However, the way a molecule vibrates—such as symmetry of stretching, scissoring, rocking, wagging or twisting—can lead to a peak not being observed. For instance, if a molecule is symmetrical and has one bond, then it will not produce a peak, but, if the molecule is asymmetrical then it will show a peak.

Capillary Electrophoresis (CE)

When there are multiple molecules that make up a solution, it is important to separate them and see what the characteristics of each molecule are—which is what capillary electrophoresis does. This separation technique relies on voltage and an electric field to separate molecules based on differences in electrophoretic mobilities that are dependent on charge, viscosity of the solvent, and size (U.S. Food and Drug Administration, 2020). Large amounts of voltage are used in CE and provide high-performance separations. It is easy to assume that large voltages can cause heating effects, but due to capillaries having a large surface area to volume ratio they are able to effectively dissipate heat, mitigating heating effects (U.S. Food and Drug Administration, 2020). When under an electric field, molecules that can be ionized become charged ions that are either positive or negative (Sutipatanasomboon, 2021). In CE, there are two electrodes—cathode and anode—that create an electric force. This force is strong and causes ions to move towards the opposite charge leading to separation. For instance, a cation would move towards the negatively charged cathode.

Nuclear Magnetic Resonance Spectroscopy (NMR)

For structure determination, NMR is valuable as it details which atoms are located next to others. This is but one application of NMR. The technique can be tailored to specific elements, such as hydrogen or carbon. Hydrogen, or proton-NMR (^{1}H-NMR) is commonly used as ^{1}H is readily available in the environment, whereas NMR that is specific to carbon uses carbon isotopes, such as ^{13}C, that are not as abundant as ^{1}H is. Placing a molecule in a magnetic field causes the nuclei of some atoms to act like small magnets and if radio frequency waves are applied, then the nuclei will resonate at specific frequencies. From here, the frequencies are measured and form an NMR spectrum. The higher the radio frequency, the higher the resolution and separation of peaks are.

Objectives of Study

The purpose of this study was two-fold. The first objective was to develop a purification and separation technique that could successfully elute potential UV resistant molecules in the powder. The second goal of the project was to characterize and elucidate the structures of any UV resistant molecules that were separated from the powder. The characterization part of the work

included finding the polarity of the powder, while elucidating the structure comprised of finding the functional groups present in the UV resistant molecules.

METHODS AND MATERIALS

Sample Collection

The Trembling Aspen Tree powder was collected in June 2022 at a site at Lac Du Bois, Kamloops, BC, Canada. The site was outside of the protected area—samples were collected without scraping off significant amounts of bark or other parts of the tree that could cause it to degrade faster than it typically would. The bark was thin, smooth, and the distance between the powder and the bark was small. As for the powder, it appeared grey/white, and its texture was not waxy but was grainy, like sand, and is seen in Figure 2. Also, the powder was loosely held to the bark and seemed to be a surficial powder that could be removed through manual scraping.

Figure 2. Trembling Aspen tree powder appearing grey/white.

The site was approximately 20 m x 20 m and extended to the far green bushes on the left of Figure 3. The soil within the site was slightly moist, with the tallest blades of grass reaching up

to shin-length. A metal scraper and the back end of a knife were used to scrape the powder off 4 trees into a plastic bag. An issue with this method of sampling was that the powder experience static effects from the plastic bag, causing it to disperse within the air. As a solution, the bag was held up to the tree and when the powder was scraped, it fell into the bag. The powder still experienced static effects, but some of the powder fell into the bag—enough to give a mass of 2.02 grams (g).

Figure 3. Sampling site at Lac du Bois, Kamloops, BC, Canada.

Dissolution Attempts

The powder was attempted to be dissolved with 5 polar and 3 non-polar solvents along with 1 polar and non-polar mixture. The 6 polar solvents were deionized water, ethyl acetate (Fisher Scientific Co., ON, Canada), methanol (Fisher Scientific Co., ON, Canada), ethanol (Fisher Scientific Co., ON, Canada), acetonitrile (Fisher Scientific Co., ON, Canada), and dimethyl sulfoxide or DMSO (Fisher Scientific Co., ON, Canada). The 3 non-polar solvents attempted were, hexane (Fisher Scientific Co., ON, Canada), tetrahydrofuran, or THF (Fisher Scientific Co., ON, Canada), and chloroform-D (Sigma-Aldrich Co LLC, Darmstadt, Germany). Deuterated chloroform was used instead of unmodified chloroform for consistency since the powder was going to be analyzed by nuclear magnetic resonance (NMR). Lastly, the polar:non-polar mixture was composed of methanol, acetonitrile, and THF (1:1:1). For each dissolution attempt, a total volume of 3 mL of the solvent was poured onto 20 mg of the powder which was in a 5 mL glass

vial. All dissolution attempts were done at 25°C and were vortexed for 5 min immediately after adding the solvent to the powder. The expected solubility for each solvent is shown in Table 1. Interestingly, chloroform-D has the lowest solubility of all the solvents used, but visibly dissolved more than any of the other solvents. This discrepancy could be due to chloroform's polar nature and tendency to dissolve both polar and non-polar solutes, hence, appearing like it dissolved more of the powder than other solvents which primarily dissolve either polar or non-polar solutes.

Table 1. Expected solubilities at 25°C for each solvent (n = 9).

Solvent Type	Mass (mg)	Mass of Solvent (g)	Expected Solubility (mg/100 g)
Methanol	17	2.373	716.4
Ethanol	18	2.367	760.5
Acetonitrile	16	2.358	678.5
Dimethyl sulfoxide	21	3.300	636.4
Ethyl acetate	25	2.706	923.9
Hexane	19	1.977	961.1
THF	20	2.667	749.9
Chloroform-D	20	4.500	444.4
Mixture (1:1:1)	18	2.366	760.8

Note: The mass of the solvent was calculated by multiplying the volume of solvent used and the density of the solvent at 25°C.

Sample Preparation/Purification

Samples were prepared two different ways. The first sample was prepared by dissolving the raw powder in $CDCl_3$ and heating it to 40°C to assist with dissolution. This sample was then filtered using a glass filter. The second method stems from purifying the sample, which had to first be prepared for flash column chromatography. However, the typical flash column chromatography method was not suitable for the solvent of choice—which was $CDCl_3$—since it is stronger than traditional solvents such as methanol (Merck, 2021; Techiescientist, n.d.). Instead, a dry-loading technique for flash column chromatography was used. To prepare a sample for dry-loading, a solvent mixture had to be used that gave retention factors of the components of interest that were between 0.2-0.3 when separated using thin layer chromatography (TLC). Given the retention factors had to be low, both polar and non-polar mobile phases were used of varying ratios of hexane, ethyl acetate, THF, ethyl alcohol, 2-propanol, and methanol. This was done because the polarities of the components of the powder were not clear even after dissolution attempts.

Though a majority of the powder dissolved in $CDCl_3$ which is considered to be non-polar, the nature of $CDCl_3$ causes it to dissolve some polar compounds, making it appear that more of the sample was dissolved. Since both non-polar and polar components could be dissolved, assuming the powder consists of polar or non-polar would be accurate. Before applying the sample to TLC plates, it was purified using a Rotovap which evaporated the methanol that partially dissolved the sample. Methanol was used instead of deuterated chloroform to conserve resources and prevent solvent waste since only the mobile phase needed to be optimized. There was approximately 0.5000 g of sample dissolved in 25.0 mL of solvent, filtered, and transferred into a 50 mL round bottom flask. The sample was subjected to the Rotovap for 30 min and then 3 mL of methanol were added to the small volume of liquid that remained in the round bottom flask to increase the volume for TLC spotting. For the other mobile phases, the same procedure was followed. Each mobile phase had a final volume of 200 mL. The polar solvent mixtures did not give the desired retention factors, but, a non-polar solvent mixture of hexane and ethyl acetate (4:1) did. The dry-loading technique used this mobile phase.

To setup the dry-loading technique, 100 mg of sample was dissolved in 12.5 mL of deuterated chloroform, heated, filtered, and transferred to a 25 mL round bottom flask that was placed onto a Rotovap. After evaporation, 2 g of silica gel (Sigma-Aldrich Co LLC, Darmstadt, Germany) was added to the flask and mixed until the solution had a slush consistency. The solution was evaporated util the slush consistency turned into the same consistency as silica gel. At this point, the colour changed from white to yellow. Then, to a 60 mL flash column which had cotton in the narrow bottom of the column, enough silica gel was added to the column to fill the bottom up to 5 cm. Then, the yellow silica gel was added onto the white silica gel and 2-3 cm of the mobile phase was added. To this, 2-5 mm of sand (Fischer Scientific Co., ON, Canada) was added. Once the dry-loading technique was set, the mobile phase was run through twice and fractions were collected every 2 mL, giving a total of 34 mL being collected.

Instruments and Parameters

Cell Imaging Microscopy

Before any analytical and spectroscopic analysis was done, the powder was viewed under an EVOS M5000 (Life Technologies Inc., Burlington, ON, Canada) imaging microscope and

stained using Toluidine Blue (Sigma-Aldrich Co LLC, Darmstadt, Germany). The parameters for the microscope are seen in Table 2.

Table 2. Parameters for EVOS M5000 Cell Imaging Microscope.

Parameters	
Illumination	LED light cubes
Contrast Methods	Epifluorescence and transmitted light
Objective Turret	5-position control
LCD Display	18.5 in. high-resolution
Camera	3.2 MP, monochrome CMOS camera (2048 x 1536 pixels)
Pixel resolution	3.45 μm

Capillary Electrophoresis

With the sample purified from flash column chromatography, the purified fractions were analyzed using a Beckman Coulter P/ACE^{TM} MDQ capillary electrophoresis (Beckman Coulter Inc., Fullerton, CA, USA) instrument that had an ultraviolet detector. Data was acquired and processed using 32Karat software. In addition, a 60 cm (52 cm to the detector) x 50 μm uncoated fused-silica capillary was used. The separations and UV detection of the purified fractions were done by rinsing the capillary with 0.1 M NaOH, 18 MΩ water, and an organic buffer or background electrolyte composed of 60% acetonitrile and 5 mM of NaOH. The NaOH and buffer rinses were done for 4.00 min at 20 psi, while the 18 MΩ water rinse was done at 20 psi for 1.00 min. When injecting the sample, the pressure was 1 psi and was injected for 5.0 sec. Once the sample was injected, the analysis time was set for 20.0 min at a voltage of 20.0 kV with a 0.17 min ramp. Between each injection the capillary was washed with 0.1 M NaOH (4.00 min), followed by 18 MΩ water (1.00 min) then lastly the run buffer (4.00 min). The instrument parameters are seen in Table 3.

Table 3. Instrument parameters for PA 800 CE.

Parameters	
Voltage	20.0 kV
Rinse Pressure	20.0 psi
Inject Pressure	1.0 psi
Detector	UV
Wavelength	214 nm
Data Rate	4 Hz
Absorbance Signal	Direct
Polarity	Normal
Current	300 μA (maximum)
Cartridge and Sample Storage Temperatures	25.0°C
Peak Detection Threshold	2
Peak Detection Width	9

^{1}H-NMR

The ^{1}H-NMR spectra were acquired with a Bruker Avance III Ultrashield 500 MHz NMR spectrometer (Bruker Co., MA, USA) using $CDCl_3$ as the solvent and residual protons as an internal reference. When pouring samples into the NMR tubes, approximately 1-2 mL were used. The operating parameters of the NMR are in Table 4.

Table 4. Spectrometer parameters of NMR.

Parameters	
Nucleus	^{1}H
Pulse Width	7.00 μs
Power	17.445 W

Note: 'Observe' and 'decouple' parameters are the same.

FTIR

Infrared spectra were obtained using a PerkinElmer Spectrum Two (UATR Two) FTIR spectrometer (PerkinElmer Analytical and Enterprise Solutions, CT, USA). The samples were only run in a powder form, which was often done by absorbing a liquid sample onto silica gel. Blank solutions depended on the matrix of the sample, which was either $CDCl_3$, hexane:ethyl acetate, silica gel, or a mixture of some or all. The instrument parameters of the FTIR are in Table 5.

Table 5. Instrument parameters of FTIR.

Parameters	
Abscissa Units	Wavenumber
Ordinate Units	%T (Transmittance)
Wavenumber Range	450-4000 cm^{-1}
Accumulations	4 scans
Resolution	4 cm^{-1}
Crystal	Diamond
Source	MIR (8000-30) cm^{-1}
Beamsplitter	OptKBr (7800-400) cm^{-1}
Detector	LiTa03 (15700-370) cm^{-1}

UV-Vis Spectrometry

It should be noted that UV-Vis spectrometry was also performed but did not yield any useful results despite significant dilution attempts, thus, it was not shown in Figure 4.

Figure 4. Flowchart of methods used in study.

RESULTS AND DISCUSSION

Cell Imaging Microscopy

The powder was viewed under a cell imaging microscope to see the cellular structure of the powder and is seen in Figure 5. From the microscopic images, it can be observed that the cells of the powder have not been fully stained with Toluidine Blue since the colour is very faint. This indicates that the walls of the cells comprising the powder are unlikely to be made primarily of cellulose (which stains purple with Toluidine Blue) or lignin (which stains blue-green with Toluidine Blue).

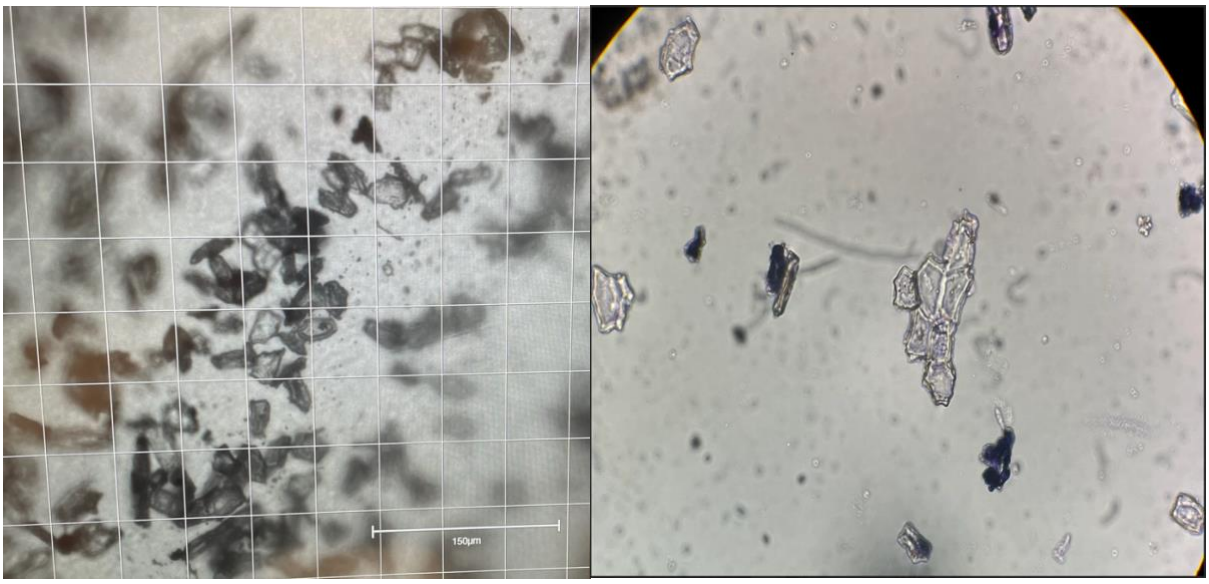

Figure 5. Microscopic images of the cells within the powder without Toluidine Blue stain (left) and with the stain (right).

Polarity

From the dissolution attempts, chloroform worked the best as it was able to visibly dissolve more of the powder than the other solvents used. The polarity of chloroform is non-polar and slightly polar due to the presence of an electronegative chlorine atom, asymmetry, and a low dielectric constant (Goyal, 2022; Ohio State University, n.d.; Techiescientist, n.d.). Due to the complex polarity of chloroform, it was difficult to classify the powder as either polar or non-polar based on the principles of dissolution. So, information from the other dissolution attempts was used to get a finer picture of the powder's polarity. For instance, the powder did not dissolve in water, but slightly dissolved in methanol and DMSO which are stronger polar solvents than water as seen with the expected solubilities in Table 1. This property is exhibited by polar oils: insoluble in water but soluble in stronger polar solvents (O'Lenick, 2008). However, polar oils are expected to dissolve more in methanol and DMSO than they do in deuterated chloroform since the former compounds are more polar than the latter. The *Populus tremuloides* tree powder did not follow this pattern. This discrepancy may be due to the ability of deuterated chloroform to dissolve non-polar compounds which may compose a significant amount of the powder. Thus, the powder would appear to be more dissolved since not only are some of the polar components being dissolved, but also the non-polar components are too, which methanol and DMSO cannot do.

The retention factors obtained (Table 6) with thin layer chromatography plates support the hypothesis that the powder is like a polar oil. Since the TLC plates had a polar stationary phase made of silica gel, the mobile phases were created as mixtures of polar and non-polar solvents to maximize the chances of observing UV resistant molecules in the powder. For mobile phases such as THF and hexane: 2-propanol (1:1), only one spot was observed at 10.1 cm and 7.5 cm, respectively, which is close to the migration distance of the methanol standard. This indicates that no components in the powder were separated when using either mobile phase, or the components were separated but they travelled off the TLC plate. If the latter reasoning is true, then it would suggest that the components in the powder were of similar polarity to the mobile phase since they will have been more attracted to the mobile phase and have travelled with it.

When using the ethyl alcohol:hexane (1:1) mobile phase, three components were separated with distances of 1.0 cm, 7.8 cm, and 14.0 cm, one of which belongs to the methanol standard which was the dot at 1.0 cm. The other two components had very large retention factors because they travelled with the mobile phase instead of being attracted to the polar stationary phase, thus, these components would be non-polar. Whether the two components were UV resistant molecules or other molecules in the powder remains unknown. This uncertainty is applicable to the THF and hexane:2-propanol mobiles phases too.

So, a mobile phase that showed multiple separated components was sought after since it had a higher likelihood of successfully separating some of the UV resistant molecules. In fact, the hexane:ethyl acetate mobile phase showed exactly that. The ethyl acetate:hexane (1:1) mobile phase separated five components in the powder with distances of 2.5 cm, 7.0 cm, 8.0 cm, 9.0 cm, and 11.8 cm. The first component belongs to the methanol standard which had a migration distance of 2.0 cm. The components at 7.0 cm, 8.0 cm, 9.0 cm, and 11.8 cm had retention factors of 0.41, 0.47, 0.53, and 0.69. These retention factors are of an intermediate polarity, indicating that the polarity of the components are between polar and non-polar. Interacting with the stationary phase equally with the mobile phase will cause separated components to travel half the distance of the solvent front, so they will not remain close to the bottom of the plate or travel the entire distance of the plate with the mobile phase. This result supports the classification of the powder as being between a polar oil and a non-polar compound.

When the same mobile phase was used but with a majority of non-polar hexane (4:1), more compounds were separated with distances of 4.2 cm, 5.0 cm, 5.2 cm, 6.0 cm, 6.5 cm, 7.5 cm, 9.5 cm, 10.5 cm, 11.0 cm, and 12.0 cm. Of these distances, the 7.5 cm compound is the methanol standard which travelled 7.8 cm. The components at 9.5 cm, 10.5 cm, and 11.0 cm exhibit the same intermediate polarity as the components in the 1:1 ethyl acetate:hexane mobile phase since they have close retention factors. However, the compounds that travelled 4.2 cm, 5.0 cm, 5.2 cm, 6.0 cm, and 6.5 cm have low retention factors of 0.25, 0.29, 0.31, 0.35, and 0.38, respectively. Low retention factors suggest that the components are polar since they are interacting closely with the polar stationary phase. On the other hand, the component at 12.0 cm had a large retention factor of 0.71. A large retention factor implies that the component is non-polar.

The combination of polar, intermediate polarity, and non-polar compounds in the powder is expected and supports the powder being between a polar oil and a non-polar compound. Since the powder has compounds with a wide range of polarities, it supports the explanation of deuterated chloroform dissolving more of the powder than methanol and DMSO. Deuterated chloroform has an intermediate polarity so it can dissolve a wide range of compounds and since the components comprising the powder that were separated with TLC had broad polarities, $CDCl_3$ would be able to dissolve these components—giving the appearance of a more dissolved solution than the strongly polar solvents methanol and DMSO could.

Table 6. Migration distances and retention factors for TLC plate characterizations of the dissolved powder.

TLC Plate Mobile Phase	Powder Migration Distances (cm)	Standard Migration Distance (cm)	Solvent Front Distance (cm)	Powder Retention Factors	Standard Retention Factor
4:1 hexane:ethyl acetate	4.2; 5.0; 5.2; 6.0; 6.5; 7.5; 9.5; 10.5; 11.0; 12.0	7.8	17.0	0.25; 0.29; 0.31; 0.35; 0.38; 0.44; 0.56; 0.62; 0.65; 0.71	0.46
1:1 ethyl alcohol:hexane	1.0; 7.8; 14.0	1.0	15.0	0.07; 0.52; 0.93	0.07
1:1 ethyl acetate:hexane	2.5; 7.0; 8.0; 9.0; 11.8	2.0	17.0	0.15; 0.41; 0.47; 0.53; 0.69	0.12
1:1 hexane: 2-propanol	7.5	7.8	15.5	0.48	0.50
THF	10.1	12.0	13.0	0.78	0.92

UV Detection and Number of Potential UV Molecules in Powder

Before subjecting the purified fractions of the sample to spectroscopic techniques and analytical instruments, the principle of UV resistance that this work is based on had to be tested. A common technique to test for UV resistance would be UV-Vis spectrometry, as any molecules that absorb UV light will show up as a broad spectrum. However, when the purified samples were run by UV-Vis spectrometry, they showed up as narrow peaks instead of broad ones. Typically, this issue is fixed by dilution, but in this case, not even diluting the purified samples by 10^5X made the peaks broad. The narrow peaks could be due to the matrix of the samples masking any UV resistant molecules, hence, the narrow peaks might belong to components in the solvent mixture. To overcome the issue of the solvent masking the UV resistant molecules, a separation technique with a UV detector needed to be used as it would further separate the UV resistant molecules from the solvent components while detecting if the molecules absorb UV light. So, CE was chosen.

There were 17 purified fractions that were run on CE, each with 500 μL of solution, along with 3 blanks that were $CDCl_3$, hexane:ethyl acetate (4:1), and a mixture of $CDCl_3$ and hexane:ethyl acetate (4:1). The identification of potential UV resistant molecules in the purified fractions are summarized in Table 7.

Table 7. Summarized results of CE analysis showing potentially new UV resistant molecules in purified fractions at specific migration time intervals.

Fraction	Volume (mL)	Migration time (min)								
-	-	0-2	2-4	4-6	6-8	8-10	10-12	12-14	14-16	16-18
A	2	X	X	✓	X	X	X	X	X	X
B	4	X	X	✓	X	X	X	X	X	X
C	6	X	X	✓	X	X	X	X	X	X
D	8	X	X	✓	X	X	X	X	X	X
E	10	X	X	X	X	X	X	X	X	X
F	12	X	X	✓	X	X	X	X	X	X
G	14	X	X	X	X	X	X	X	X	X
H	16	X	X	✓	X	X	X	X	X	X
I	18	X	X	✓	X	X	X	X	X	X
J	20	X	X	X	X	X	✓	X	X	X
K	22	X	X	X	✓	X	X	X	X	X
L	24	X	X	X	X	X	X	X	X	X
M	26	X	X	✓	X	X	✓	X	X	X
N	28	X	X	✓	X	X	X	X	X	X
O	30	X	X	X	X	X	X	X	X	X
P	32	X	X	✓	X	X	X	X	X	X
Q	34	X	X	✓	X	X	X	X	✓	X

Note: '✓' indicates the presence of a new peak from a potential UV resistant molecule, while 'X' indicates the absence of a peak from a potential UV resistant molecule.

CE Electropherogram Discussion

Starting with the blank samples, Figure A1 shows the $CDCl_3$ blank. The large peak at 3.5 min with a peak area of 686386 belongs to a major impurity—such as water—in the $CDCl_3$ solvent mixture since it is the strongest, and the other smaller peaks on the right side of Figure A1 may be other contaminants or noise. The latter is more reasonable based on the absence of baseline resolution for peaks on the right side of Figure A1.

Figures A2 and A2(a) shows the hexane:ethyl acetate (4:1) blank. Since this blank is a combination of two compounds along with any contaminants from both solvents, the electropherogram is expected to contain many peaks, which is seen. The peak that belongs to the major impurity in the hexane:ethyl acetate solvent mixture may be the large peak at 10.8 min that

has a peak area of 118317. The other peaks are a mixture of both, impurities from the hexane and ethyl acetate stock solution and background noise.

Figure 6 shows the $CDCl_3$ and hexane:ethyl acetate (4:1) blank mixture. What is expected in the electropherogram from this mixture is that the main peaks in Figures A1 and A2 for $CDCl_3$ and hexane:ethyl acetate (4:1) should be present—but they were not. The only peak that was of significance in Figure 6 was the peak at 3.5 min that had a peak area of 16152. Since this peak has a close migration time to the impurity peak in Figure A1, it is reasonable to conclude that these peaks belong to the same impurity. Interestingly, there is another peak that is being masked by the impurity peak and has a peak area of 19715, which could belong to impurities seen in Figure A2 that are co-migrating with other contaminants. The peak areas for both peaks in Figure 6 are lower than their associated peaks in Figures A1 and A2 potentially due to background noise or signal suppression.

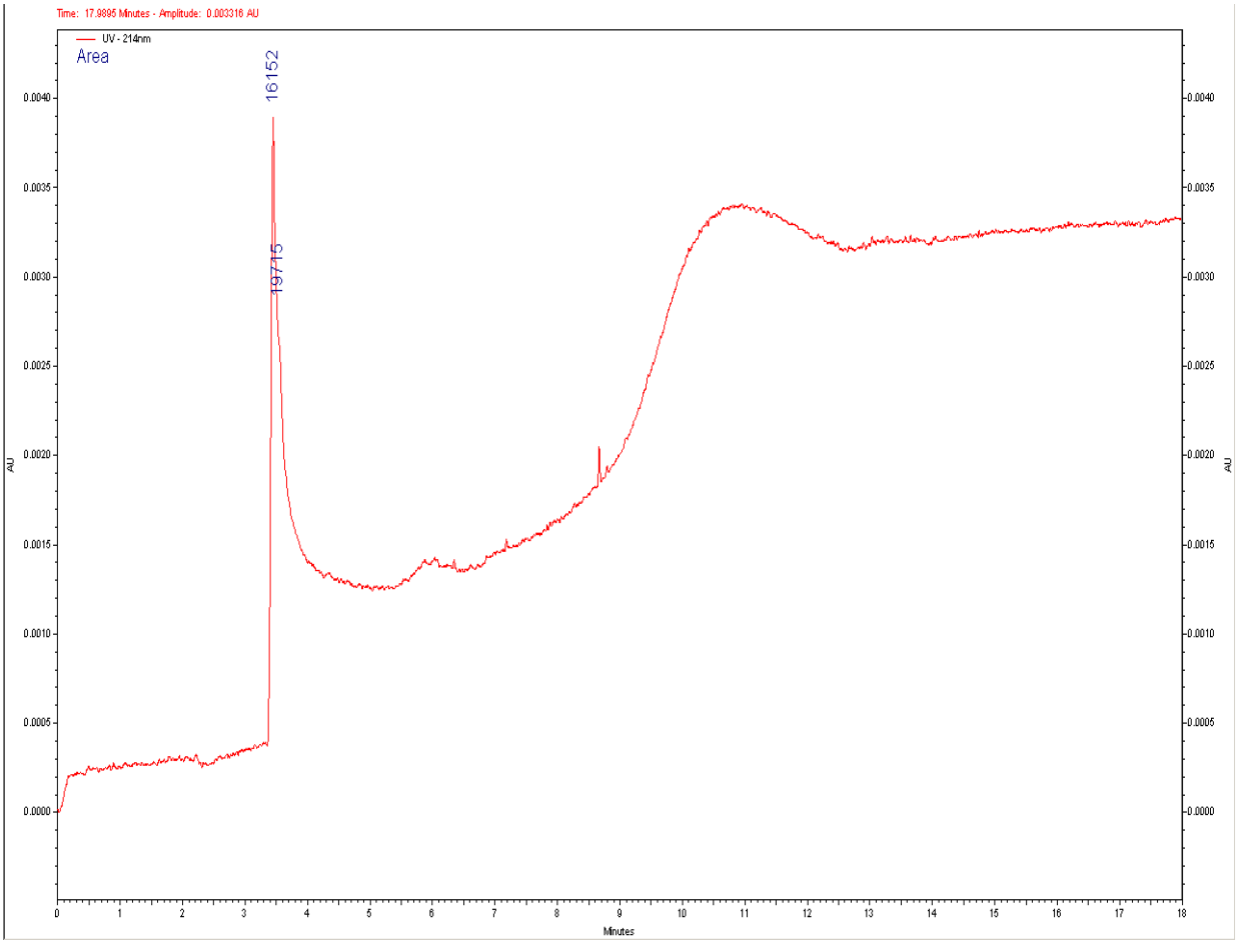

Figure 6. Electropherogram of $CDCl_3$ and hexane:ethyl acetate (4:1) mixture blank.

Figure 7 shows the raw powder dissolved in $CDCl_3$ and heated. The large peak at 4.0 min (peak area = 2040504) most likely belongs to the impurity peak in the $CDCl_3$ blank, but it could be co-migrating with a UV resistant molecule. The peak at 11.4 min (peak area = 46059) could be a potential UV molecule. Since the peak is relatively larger than the other peaks in the electropherogram, it might be one of the main UV resistant molecules in the powder. The other peaks could also belong to UV resistant molecules, but the sample concentration may be too dilute, or the molecules could have degraded significantly making their peaks very small.

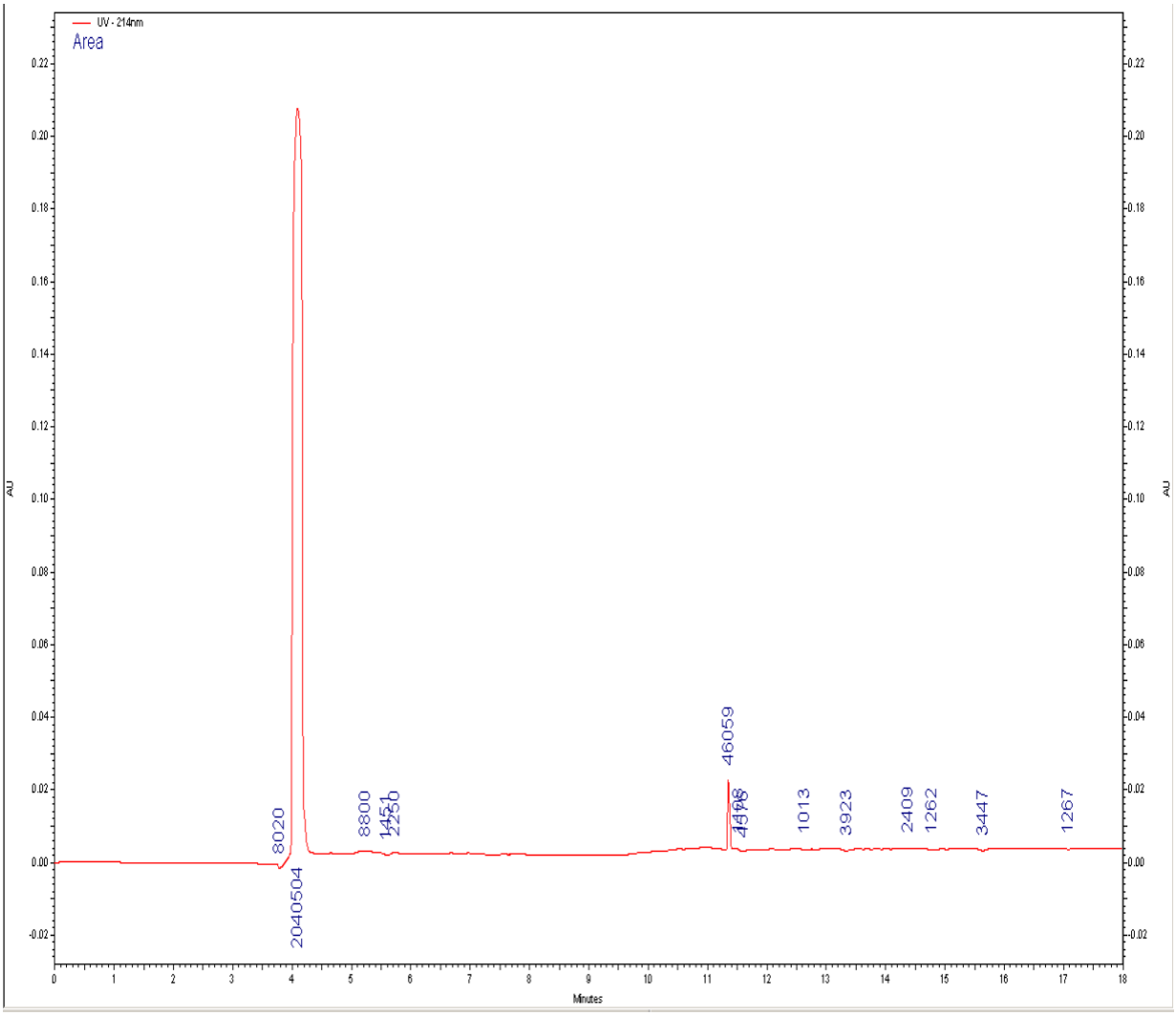

Figure 7. Electropherogram of raw powder dissolved in $CDCl_3$ and heated.

In Figure A3, an electropherogram of the 2 mL purified fraction is shown. The large peaks at 4.5 min (peak areas = 32164; 15379; 6970) could belong to potential UV resistant molecules that are co-migrating with each other. Due to the background noise and lack of baseline

resolution—which could be due to the high concentration of mobile phase—it is difficult to be sure which peaks may belong to UV resistant molecules and which are from the blanks.

The separated components in the 4 mL purified fraction are seen in Figure A4. Between Figures A3 and A4, there is more separation and the shoulder present at 4.8 min (peak area = 6970) in Figure A3 is separated with acceptable resolution in Figure A4 and can be seen as two peaks instead of one. These peaks can also belong to UV resistant molecules in the powder as they disappear in the later purified extractions. If the two peaks did belong to the matrix components, then they would be in all the electropherograms and not a select few since the matrix is the same for all of the purified fractions. The two peaks to the left of the electropherogram in Figure A3 were detected in Figure A4 at 1.5 min (peak area = 1234) and 1.8 min (peak area = 685). These two peaks are likely impurities from the blanks since they were not detected in Figure 7, which should have detected all the potential UV resistant molecules present in the powder.

The electropherogram of the 6 mL purified fraction is in Figure A5. The peak at 1.5 min that was present started to disappear. The same trend is seen with the peak at 4.8 min A new peak appeared at the end of the run at 17.5 min (peak area = 1929) which is seen in the Figure A1 blank and could be an impurity.

In Figure A6, the 8 mL purified fraction is seen. The peak at 1.5 min in Figure A5 disappeared, supporting how that peak might be an impurity since it may have been fully removed as it does not reappear in any of the later electropherograms. The peak at 5.0 min (peak area = 14959) does appear in Figure A5 and in some of the later electropherograms, thus, it could be a residual contaminant from the matrix solution. The peak at 17.5 min in Figure A5 is disappearing in Figure A6, also suggesting that it might be an impurity. New peaks appeared between 16.0 min to 17.0 min (peak areas = 599, 874, and 1498) which could be UV resistant molecules, but it is difficult to make this claim based on their abundance.

The 10 mL purified fraction is shown in Figure A7. The peak at 1.5 min in Figure A4 reappeared in Figure A7 at the same migration time with a peak area of 4359. Two new peaks appeared at 6.1 min (peak areas = 6278 and 18518), along with two smaller peaks at 11.5 min (peak areas = 1249 and 1343). These peaks are difficult to interpret as they are small and could be residual contaminants from the mobile phase mixture. There also seems to be an additional peak

at 17.0 min, where in Figure A6 there was only one peak. This second peak could be from the mobile phase or due to background noise.

Figure A8 shows the 12 mL purified fraction electropherogram. The peak at 1.5 min is still present and shows up as two peaks (peak areas = 1342 and 3273). What is most likely is that these peaks are residual contaminants peak based on their broad peak shape. Also, there is a new potential UV resistant molecule peak in Figure A8 and 5.3 min (peak area = 40228) as this peak is narrow and relatively large. At the end of the electropherogram there are multiple peaks which could be from background noise or instability of the matrix solution.

Figure A9 shows the 14 mL purified fraction's electropherogram. This electropherogram looks similar to Figure A8, but without the expected background noise peaks. The peak at 5.3 min that is present in Figure A8 disappeared but there are two peaks (peak areas = 2418 and 621) that should be ignored since they are small and likely impurities.

Figure A10 shows the electropherogram of the 16 mL purified fraction. The peaks are similar to the ones in Figure A9, but there appears to be a new peak at 5.3 min (peak area = 8226) which could be another UV resistant molecule since it is not seen in the blanks.

Figure A11 shows the electropherogram of the 18 mL purified fraction. There is a new peak at 13.7 min (peak area = 12552) that is too small so it is not a potential molecule but instead is a contaminant. However, the peak at 5.6 min (peak area = 12552) could be a potential UV resistant molecule and may be the molecule in Figure A10 that showed up approximately at the same migration time, or it could be another peak that co-migrated.

Figure A12 shows the electropherogram of the 20 mL purified fraction. The shoulder peak at 4.5 min (peak area = 2186) has gotten closer to the largest peak and is likely to be an impurity that co-migrated with the large peak and has now slightly separated. In addition, a new peak appeared at 10.2 min (peak area = 1389), and is relatively larger than the other potential UV resistant molecule peaks, so, it is likely that this peak belongs to a UV resistant molecule.

Figure A13 shows the electropherogram of the 22 mL purified fraction. The impurity shoulder peaks are still present in Figure A13, but there is a new peak at 6.3 min (peak area = 17747) and it could be a UV resistant molecule. At 15.0 min, two peaks appeared (peak areas =

170 and 9081) which are relatively small and reappear in the later figures, so they are residual contaminants from the matrix solution.

Figure A14 depicts the electropherogram of the 24 mL purified fraction. The peaks at 1.5 min, reappeared, which supports how they might be residual contaminants that occasionally get into the fractions since there is no pattern to the appearance.

Figure A15 depicts the electropherogram for the 26 mL purified fraction. This electropherogram has many new peaks that were not seen in the other figures. New smaller peaks appeared at 6.3 min (peak area = 1116), 7.1 min (peak area = 1719), 7.6 min (peak area = 4174), 10.4 min (peak areas = 20884 and 31830), 11.3 min (peak area = 574), 11.5 min (peak area = 2470) and 12.5 min (peak area = 1875). Of these peaks, the ones at 10.4 min are likely to be UV resistant molecules since their peaks are relatively larger than others. Also, the peak at 4.4 min (peak area = 327597) could also be a UV resistant molecule as it has not appeared in any of the prior electropherograms and is large.

Figure A16 shows the 28 mL purified fraction's electropherogram. The 10.5 min peak is small so it is an impurity from the matrix solution. There is also a peak at 16.1 min (peak area = 1003) that based on its size it likely to be an impurity.

Figure A17 shows the electropherogram of the 30 mL. There is a peak that appeared at 1.9 min (peak area = 3165) and is a contaminant since it is broad.

Figure A18 shows the electropherogram for the 32 mL purified fraction. A peak appeared at 8.7 min (peak area = 876), and since it is small it is an impurity. The peak at 4.7 min (peak area = 14532) is likely to be a potential UV resistant molecule since its size is relatively larger than other peaks.

Figure 8 shows the 34 mL purified fraction's electropherogram. There is a new peak at 6.0 min (peak area = 35708), and since it is large it could be a UV resistant molecule. Upon zooming in on this peak as seen in Figure 8a, there are two doublet peaks that indicate the presence of 4 UV resistant molecules. The peak at 8.9 min has a peak area of 536 and is thus a contaminant. Also, a new peak appeared at 14.5 min (peak area = 4794). This peak could be a molecule with UV resistance since the size is larger than other peaks, and the peak showed up as narrow.

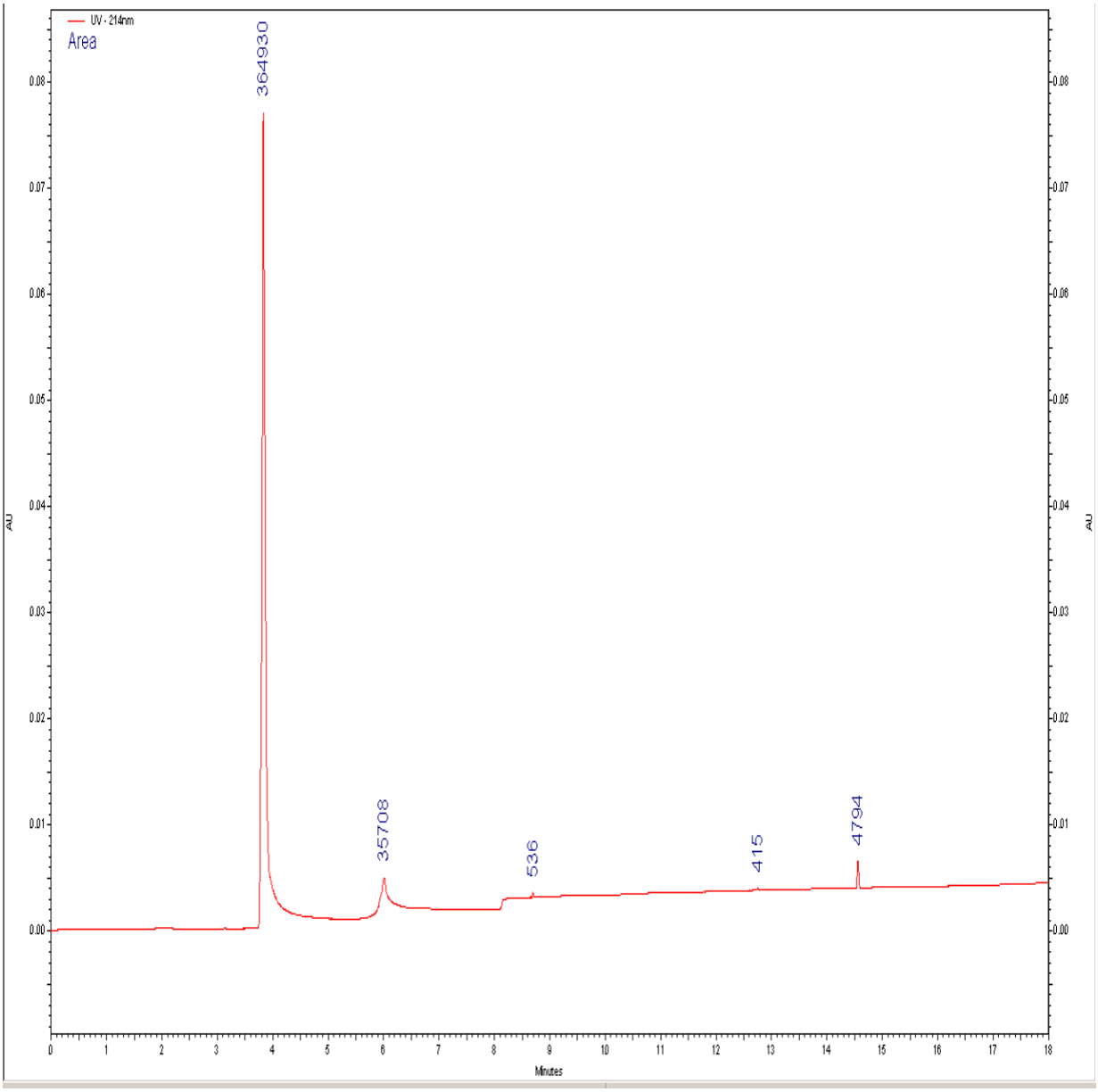

Figure 8. Electropherogram of 34 mL purified fraction in $CDCl_3$ and hexane:ethyl acetate (4:1).

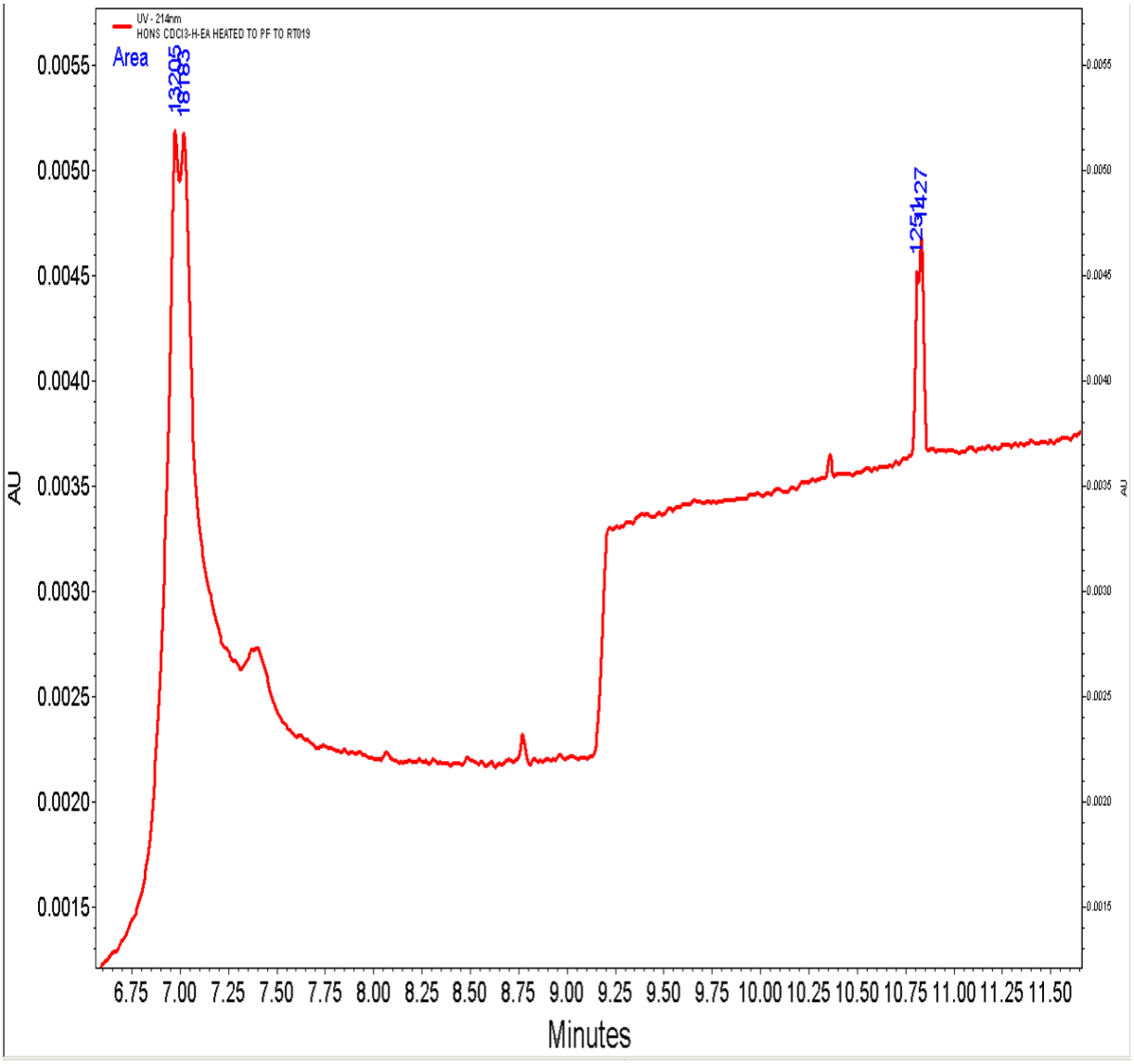

Figure 8a. Zoomed electropherogram of 34 mL purified fraction in $CDCl_3$ and hexane:ethyl acetate (4:1) from 6.75 min to 11.50 min.

Structure Elucidation

When analyzing the purified fractions on NMR and FTIR, useful results were not obtained as the spectra appeared either exactly like the blank, or messy making it difficult to interpret. This may be due to the degradation of the UV resistant molecules, but it is more likely that the purified fractions were too dilute and contained the molecules in concentrations that were lower than the limits of detections for the spectroscopic techniques. However, when the raw powder that was dissolved in $CDCl_3$ and heated was run, spectra were obtained that differed from the blanks and new peaks were visible. This sample was not as dilute as the purified fractions, supporting the

reasoning behind why the molecules in the purified fractions were not appearing. Table 8 shows the peaks and chemical shifts that were seen in the NMR spectra from Figures 9-13. The potential identities of the peaks seen in Table 8 were the peaks that fit the most with what was expected of a molecule showing UV resistance, hence, where peaks could be classified as alkene or alkyne bonds then they were classified as such. The other peaks fit with what is expected of each other, for instance, the peaks identified as –NH bonds fit with the amide classification. Despite this information, a structure could not be accurately created as the purified fractions needed to be run to determine whether the peaks are from functional groups that are on molecules, or if they are from remnants of bark or other contaminants in the raw powder.

Table 8. Peaks and chemical shifts seen in NMR spectra of raw powder dissolved in $CDCl_3$ and heated from Figures 9-13.

Chemical Shift of Peak (ppm)	Peak Splitting	Potential Identity of Peak
1.3141	Singlet	Water
2.3792	Triplet	Alkyne or –NH (primary)
2.4418	Doublet of triplets	Alkyne or –NH (primary)
3.6517	Triplet	X—C—H (where X = O)
4.0805	Doublet of triplets (low resolution)	Impurity
4.1635	Multiplet	impurity
7.0683	Singlet	Alkene
7.2896	Singlet	$CHCl_3$
7.4971	Singlet	Amide Proton
9.8071	Triplet	Aldehyde Proton

Note: Potential identities of peaks were gathered using chemical shift data from ref. 3 (Chemistry Steps, 2020).

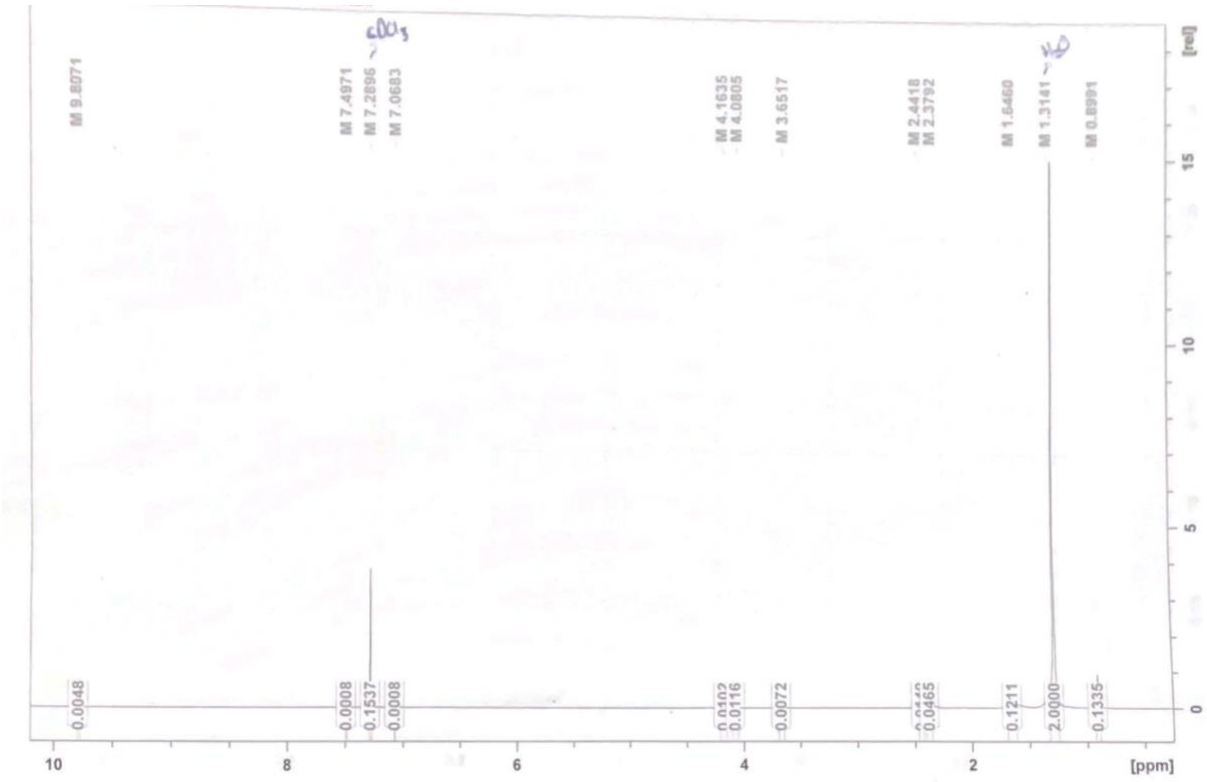

Figure 9. NMR spectrum of raw powder dissolved in $CDCl_3$ and heated.

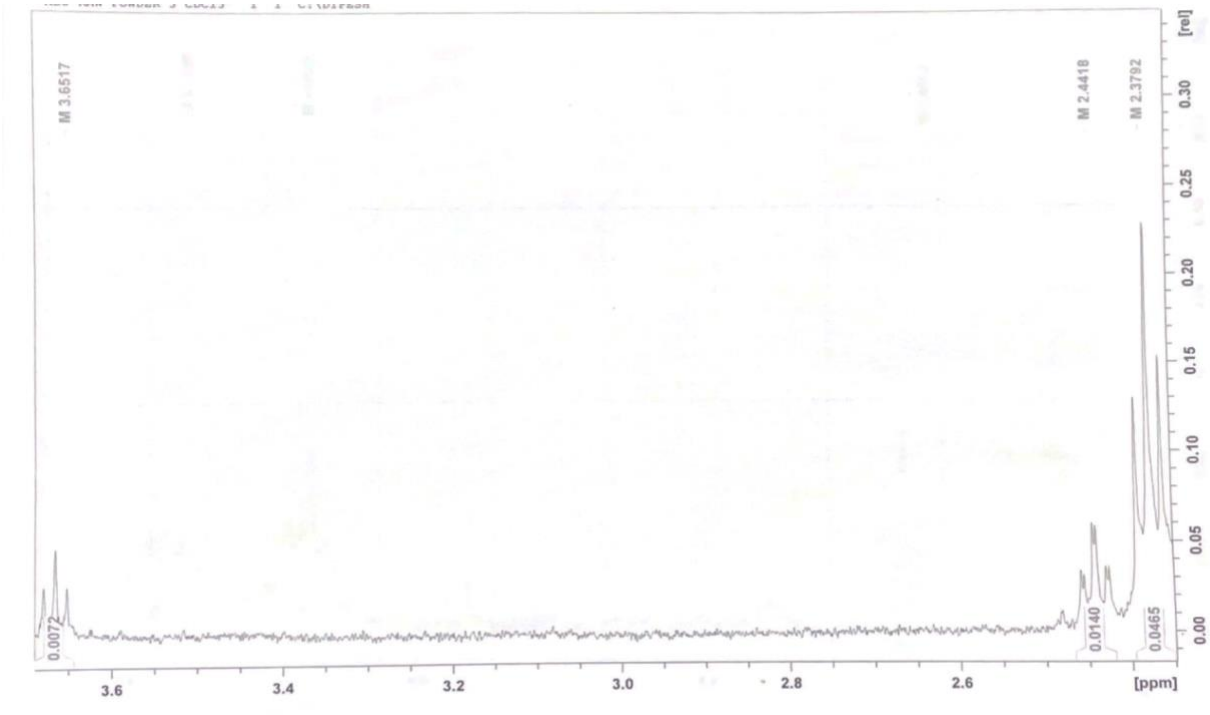

Figure 10. Zoomed NMR spectrum between 2.3 ppm to 3.65 ppm of raw powder dissolved in $CDCl_3$ and heated.

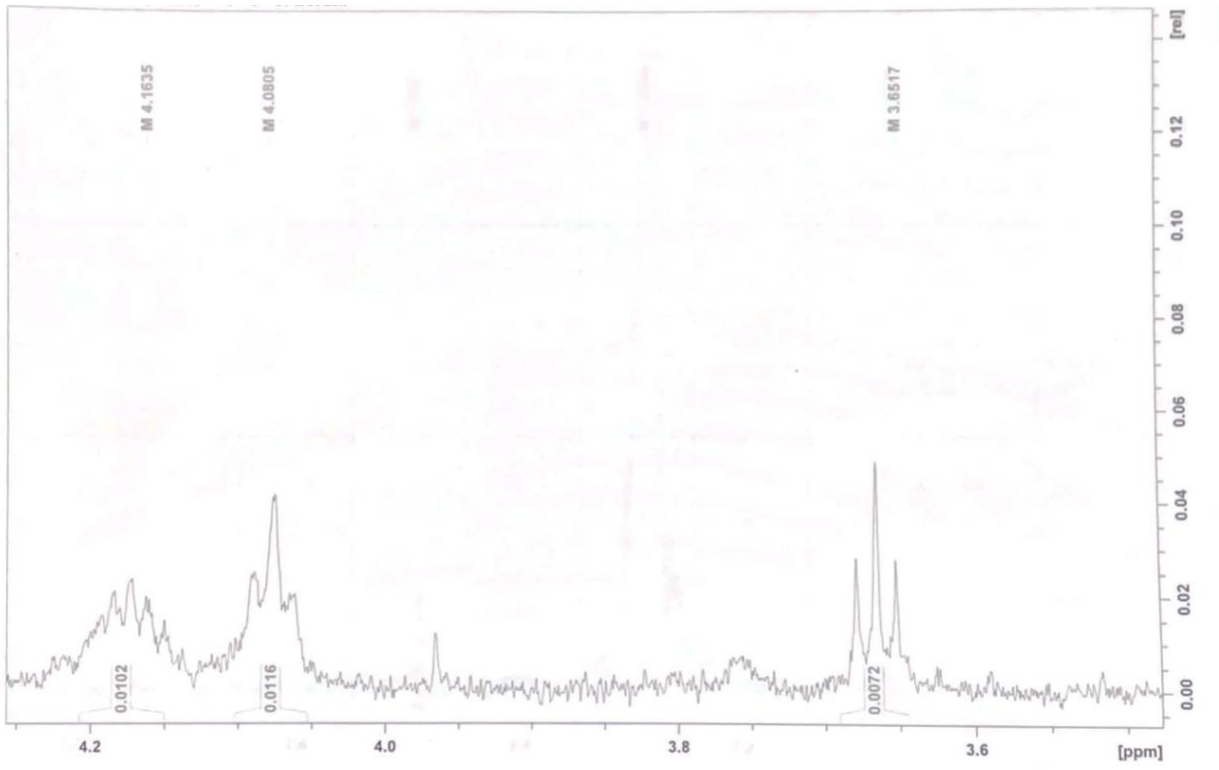

Figure 11. Zoomed NMR spectrum between 3.5 ppm to 4.2 ppm of raw powder dissolved in $CDCl_3$ and heated.

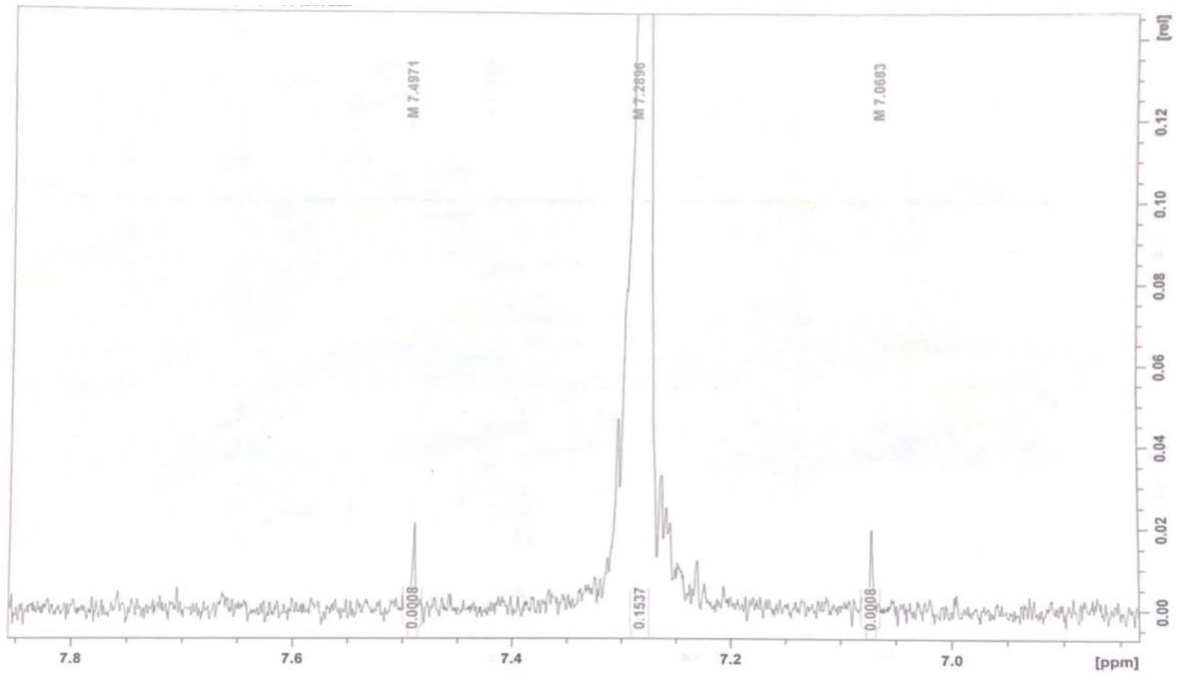

Figure 12. Zoomed NMR spectrum between 6.9 ppm to 7.8 ppm of raw powder dissolved in $CDCl_3$ and heated.

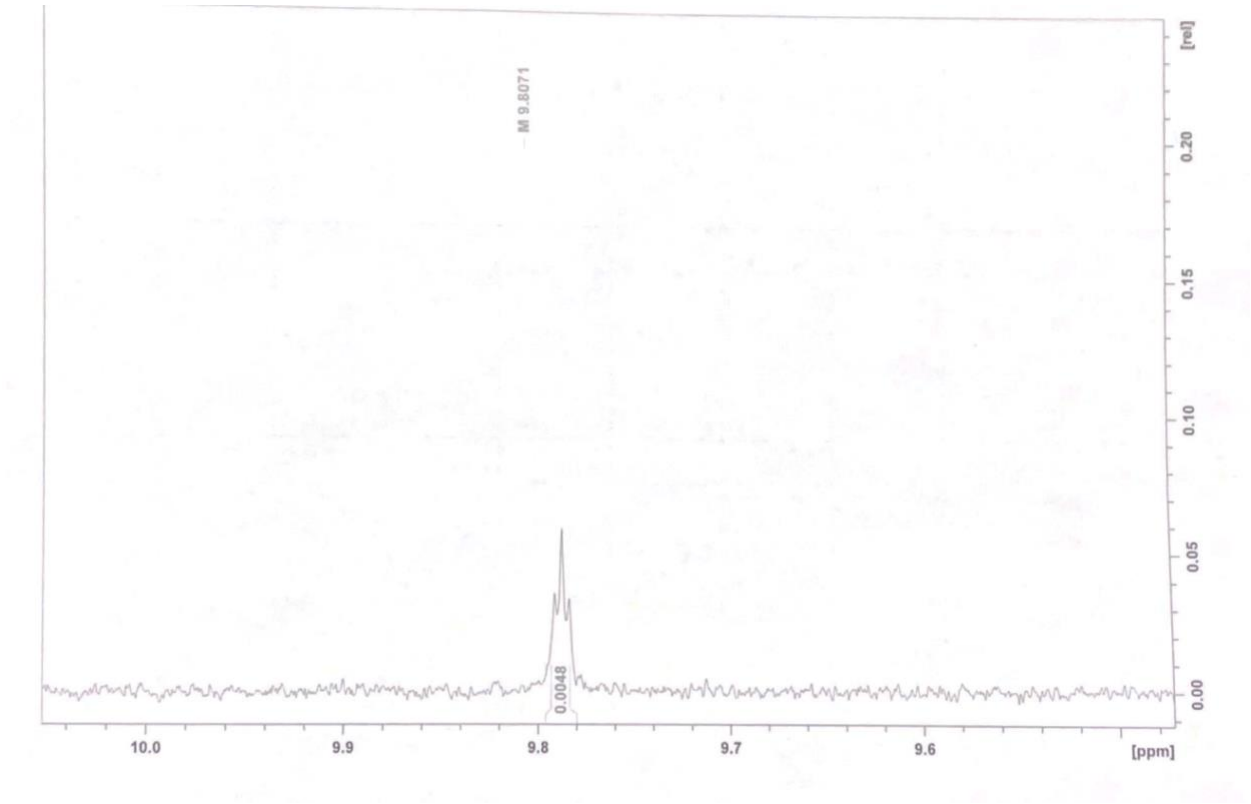

Figure 13. Zoomed NMR spectrum between 9.5 ppm to 10.1 ppm of raw powder dissolved in $CDCl_3$ and heated.

The FTIR analysis of the raw powder dissolved in $CDCl_3$, heated, and absorbed onto silica gel did not yield any significant results, as the detected peaks belong to the blanks, as seen in Table 9. However, the small peaks at 3000 cm^{-1} and 2100 cm^{-1} could be the amine nitrogen and the alkyne, respectively .[20] Due to these peaks being very small, it suggests that the sample is too dilute to be reliably detected on the FTIR, thus, this classification should not be taken as concrete.

Table 9. Peak area and height of labelled peaks in FTIR spectrum of raw powder dissolved in $CDCl_3$, heated, and absorbed onto silica gel for analysis.

Peak Number	Wavenumber (cm^{-1})	% Transmittance	Identity of Peak
1	1060.24	69.93	Silica gel
2	903.55	36.12	Silica gel
3	799.43	90.2	$CDCl_3$
4	725.32	28.54	Silica gel
5	649.94	72.38	$CDCl_3$

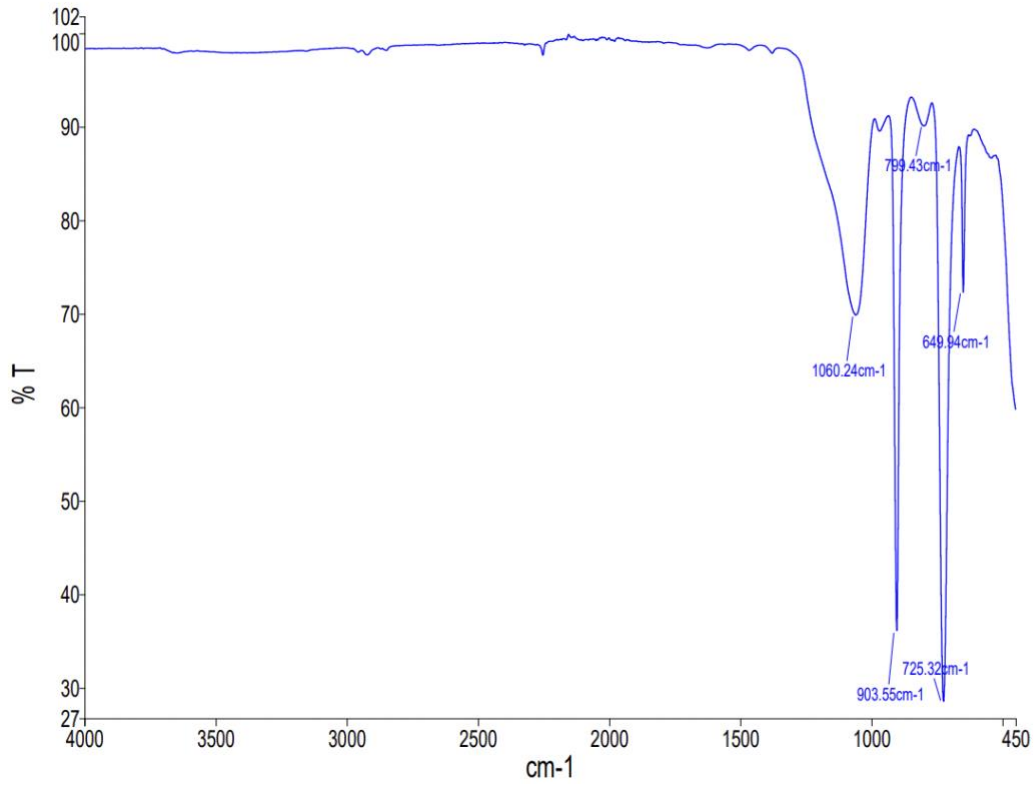

Figure 14. FTIR spectrum of raw powder dissolved in $CDCl_3$, heated, and absorbed onto silica gel for analysis.

CONCLUSION

Through sample collection, purification using flash column chromatography, and analytical and spectroscopic analysis of purified fractions and raw Trembling Aspen powder, this work has set the foundation for determining potential structures of UV resistant molecules in Trembling Aspen tree powder. The work found that there are approximately five molecules in the powder that absorb UV light, and that these molecules may have a range of functional groups such as alkenes, alkynes, amines, amides, and aldehydes, which are typical of UV resistant molecules found in commercial sunscreens. The multiple structures in the powder may have isomeric forms too, which could explain the reappearance of some peaks in the purified fractions as they may have slightly different polarities and interactions with the flash chromatography column. This work strived to act as a preliminary body of information that furthers the goal of characterizing all UV resistant molecules present in the Trembling Aspen tree powder.

Future Work

Future work entails doing two types of analysis: MALDI-MS (matrix assisted laser desorption ionization-mass spectrometry) and X-ray crystallography. The first type would allow for the masses of the UV resistant molecules to be acquired, which would narrow down how many atoms are present in each structure and the maximum number of elements in each (Broad Institute, 2010). The second type would allow for a clear identification of the structure of the UV resistant molecules which, using NMR spectra, would allow for the determination of atoms in 3D space and where each atom is connected. In addition, future work could include comparing the powder made on the shady side of Trembling Aspen during different seasons with the powder on the sunny side to see if there is a difference in the structures of UV resistant molecules in the powders.

LITERATURE CITED

Barlow, P. (2005). From cambium to early cell differentiation within the secondary vascular system. In: Holbrook, N.M., Zwienicki, M.A. (eds). *Vascular transport in plants* (pp. 279-306). Elsevier.

Borden, J. H., Wilson, I. M., Gries, R., Chong, L. J., Pierce, Jr., H. D., & Gries, G. (1998). Volatiles from the bark of trembling aspen, Populus tremuloides Michx. (Salicaceae) disrupt secondary attraction by the mountain pine beetle, Dendroctonus ponderosae Hopkins (Coleoptera: Scolytidae). *Chemoecology*, *8*(2), 69–75. https://doi.org/10.1007/pl00001806

Byjus. (n.d.). *Metabolites*. https://byjus.com/biology/metabolites/

Broad Institute. (2010, September 13). *What is Mass Spectrometry?* Broad Institute. https://www.broadinstitute.org/technology-areas/what-mass-spectrometry

Califf, R.M.; Shinkai, K. (2019). Filling in the evidence about sunscreen. *JAMA*, *321*(21), 2077–2079. doi:10.1001/jama.2019.5528

Celedon, J. M., & Bohlmann, J. (2017). An extended model of heartwood secondary metabolism informed by functional genomics. *Tree Physiology*, *38*(3), 311–319. https://doi.org/10.1093/treephys/tpx070

Chemistry Steps. (2020, February 2). *NMR Chemical Shift Values Table*. https://www.chemistrysteps.com/nmr-chemical-shift-values-table/

D'Orazio, J., Jarrett, S., Amaro-Ortiz, A., & Scott, T. (2013). UV Radiation and the Skin. *International Journal of Molecular Sciences*, *14*(6), 12222–12248. https://doi.org/10.3390/ijms140612222

Ellison, A.M.; Bank, M.S.; Clinton, B.D.; Colburn, E.A.; Elliott, K.; Ford, C.R.; Foster, D.R.; Kloeppel, B.D., Knoepp, J.D.; Lovett, G.M.; Mohan, J.; Orwig, D.A.; Rodenhouse, N.L.; Sobczak, W.V.; Stinson, K.A.; Stone, J.K.; Swan, C.M.; Thompson, J.; Von Holle, B.; Webster, J.R. (2005). Loss of foundation species: consequences for the structure and dynamics of forested ecosystems. *Frontiers in. Ecological Environ*ment, *3*(1), 479– 486.

Endress, B.A.; Wisdom, M.J.; Vavra, M.; Parks, C.G.; Dick, B.L.; Naylor, B.J.; Boyd, J.M. (2012). Effects of ungulate herbivory on aspen, cottonwood, and willow development under forest fuels treatment regimes. *Forest Ecological Management*, *276*(1), 33–40.

Evert, R.F. & Eichhorn, S.E. (2013). *Biology of Plants*. W.H. Freeman and Company Publishers.

Falcone Ferreyra, M. L., Rius, S. P., & Casati, P. (2012). Flavonoids: biosynthesis, biological functions, and biotechnological applications. *Frontiers in Plant Science*, *3*. https://doi.org/10.3389/fpls.2012.00222

Goyal, V. (2022, August 1). *Is CHCl3 Polar or Nonpolar? - Polarity of Chloroform*. Topblogtenz. https://topblogtenz.com/is-chcl3-polar-or-nonpolar/

Government of British Columbia. (n.d.). *Trembling aspen (Populus tremuloides)*. https://www.for.gov.bc.ca/hfd/library/documents/treebook/tremblingaspen.htm#:~:text=A%20slender%2C%20graceful%20tree%20with,quiver%20in%20the%20slightest%20breeze

Guerriero, G., Berni, R., Muñoz-Sanchez, J., Apone, F., Abdel-Salam, E., Qahtan, A., Alatar, A., Cantini, C., Cai, G., Hausman, J.-F., Siddiqui, K., Hernández-Sotomayor, S., & Faisal, M. (2018). Production of Plant Secondary Metabolites: Examples, Tips and Suggestions for Biotechnologists. *Genes*, *9*(6), 309. https://doi.org/10.3390/genes9060309

Hassan, S., & Mathesius, U. (2012). The role of flavonoids in root-rhizosphere signalling: opportunities and challenges for improving plant-microbe interactions. *Journal of Experimental Botany*, *63*(9), 3429–3444. https://doi.org/10.1093/jxb/err430

Impact Analytical. (2022, May 20). *Molecular Characterization*. https://www.impactanalytical.com/molecular-characterization/

Jove. (n.d.). *Capillary Electrophoresis (CE)—Protocol*. https://www.jove.com/v/10226/capillary-electrophoresis-ce

U.S. Food and Drug Administration. (2020, August 19). *Ultraviolet (UV) Radiation*. Center for Devices and Radiological Health. https://www.fda.gov/radiation-emitting-products/tanning/ultraviolet-uv-radiation

Kashian, D.M.; Romme, W.H.; Regan, C.M. (2007). Reconciling divergent interpretations of quaking aspen decline on the northern Colorado. *Frontiers in Rangeland and Ecology*, *17*(1), 1296–1311.

Lindroth, R.L.; St. Clair, S.B. (2013). Adaptations of quaking aspen (Populus tremuloides Michx.) for defense against herbivores. *Forest Ecological Management*, *299*(1), 14-21.

Mathias, J. (2015, February). *How Does FTIR Work?* Innovatech Labs. https://www.innovatechlabs.com/newsroom/672/stuff-works-ftir-analysis/

Medieval Manor Gardens. (n.d.). *Aspen, Trembling (Populus tremuloides) Alberta Native*. https://www.mmgardens.ca/product/trembling-aspen-populus-tremuloides-alberta-native/

Merck. (2021). *Solubility Rules—Solubility of Common Ionic Compounds*. Merck. https://www.sigmaaldrich.com/MX/en/technical-documents/technical-article/genomics/cloning-and-expression/blue-white-screening

Mitton, J.B.; Grant, M.C. (1996). Genetic variation and the natural history of quaking aspen. *Bioscience*, *46*(1), 25–31.

Muñoz, P., & Munné-Bosch, S. (2017). Photo-Oxidative Stress during Leaf, Flower and Fruit Development. *Plant Physiology*, *176*(2), 1004–1014. https://doi.org/10.1104/pp.17.01127

National Geographic. (n.d.). *Photosynthesis*. https://education.nationalgeographic.org/resource/photosynthesis/

Ohio State University. (n.d.). *Polarity of Solvents*. https://research.cbc.osu.edu/turro.1/wp-content/uploads/2017/02/PolarityofSolvents.pdf

O'Lenick, T. (2008, October 22). *Polar vs. Nonpolar Oils. Cosmetics & Toiletries*. https://www.cosmeticsandtoiletries.com/research/literature-data/news/21845872/polar-vs-nonpolar-oils

Omnexus. (n.d.). *UV light Resistance & Properties: Polymer Properties*. https://omnexus.specialchem.com/polymer-properties/properties/uv-light-resistance

Pang, Z., Chen, J., Wang, T., Gao, C., Li, Z., Guo, L., Xu, J., & Cheng, Y. (2021). Linking Plant Secondary Metabolites and Plant Microbiomes: A Review. *Frontiers in Plant Science*, *12*. https://doi.org/10.3389/fpls.2021.621276

Pearl, I. A., & Darling, S. F. (1959). Studies on the Barks of the Family Salicaceae. I. Tremuloidin, a New Glucoside from the Bark of Populus tremuloides. *The Journal of Organic Chemistry*, *24*(6), 731–735. https://doi.org/10.1021/jo01088a001

Plant Watch Nature Alberta. (n.d.). *Aspen Poplar*. https://plantwatch.naturealberta.ca/choose-your-plants/aspen-poplar/index.html

Rockett, C. (2019, December 12). *UV Degradation Effects in Materials – An Elementary Overview*. UV Solutions. https://uvsolutionsmag.com/articles/2019/uv-degradation-effects-in-materials-an-elementary-overview/

Sandved, K.B., Prance, G.T., & Prance, A.E. (1993). *Bark*. Timber Press.

Sigma Aldrich. (n.d.). *IR Spectrum Table*. https://www.sigmaaldrich.com/CA/en/technical-documents/technical-article/analytical-chemistry/photometry-and-reflectometry/ir-spectrum-table

Sinha, S., Sandhu, K., Bisht, N., Naliwal, T., Saini, I., & Kaushik, P. (2019). Ascertaining the Paradigm of Secondary Metabolism Enhancement through Gene Level Modification in Therapeutic Plants. *Journal of Young Pharmacists*, *11*(4), 337–343. https://doi.org/10.5530/jyp.2019.11.70

Steeley, K. G., Kuestermeyer, B., Stanton, C., Yu, J., Morabito, K., Li, D., Mello, C., Calvert, P., Tripathi, A., & Shapley, N. C. (2014). Uniform polymer particles formulated with ultraviolet protective materials for the protection of UV sensitive molecules. *Dyes and Pigments*, *105*(1), 12–22. https://doi.org/10.1016/j.dyepig.2013.12.013

St-Pierre, A., Blondeau, D., Lajeunesse, A., Bley, J., Bourdeau, N., & Desgagné-Penix, I. (2018). Phytochemical Screening of Quaking Aspen (Populus tremuloides) Extracts by UPLC-QTOF-MS and Evaluation of their Antimicrobial Activity. *Molecules*, *23*(7), 1739. https://doi.org/10.3390/molecules23071739

Sutipatanasomboon, A. (2021, April 27). *Capillary Electrophoresis*. Conduct Science. https://conductscience.com/capillary-electrophoresis/

Systems Chemistry. (n.d.). *Infrared Spectroscopy*. https://www.ru.nl/systemschemistry/equipment/optical-spectroscopy/infrared/#:~:text=The%20infrared%20portion%20of%20the,excite%20overtone%20or%20harmonic%20vibrations

Techiescientist. (n.d.). *Is CHCl3 Polar or Nonpolar?* https://techiescientist.com/is-chcl3-polar-or-nonpolar/

Teoh, E. S. (2015). Secondary Metabolites of Plants. *Medicinal Orchids of Asia*, 59–73. https://doi.org/10.1007/978-3-319-24274-3_5

The National Wildlife Federation. (n.d.). *Quaking Aspen*. https://www.nwf.org/Educational-Resources/Wildlife-Guide/Plants-and-Fungi/Quaking-Aspen#:~:text=The%20bark%20layer%20of%20quaking,from%20aspen%20groves%20in%20summer.

The Survival University. (n.d.). *Quaking Aspen*. https://thesurvivaluniversity.com/survival-tips/wilderness-survival-tips/all-about-wild-plants/wild-plant-index/quaking-aspen/

Torres, J. P., & Schmidt, E. W. (2019). The biosynthetic diversity of the animal world. *Journal of Biological Chemistry*, *294*(46), 17684–17692. https://doi.org/10.1074/jbc.rev119.006130

United States Department of Agriculture. (n.d.). *Plant Guide*. https://plants.usda.gov/DocumentLibrary/plantguide/pdf/cs_potr5.pdf

University of Colorado Boulder. (2015, October 20). *The Mystery of Aspen Powder*. https://www.colorado.edu/ebio/2015/10/20/mystery-aspen-powder#:~:text=The%20accumulated%20layer%20of%20bark,cambium%20to%20reach%20the%20chlorenchyma

University of Minnesota. (n.d.). *Quaking Aspen—Populus tremuloides*. https://trees.umn.edu/quaking-aspen-populus-tremuloides

University of Saskatchewan. (2021, April 30). *Trembling Aspen*. https://gardening.usask.ca/articles-and-lists/articles-plant-descriptions/trees/trembling-aspen.php

Valenta, K., Dimac-Stohl, K., Baines, F., Smith, T., Piotrowski, G., Hill, N., Kuppler, J., & Nevo, O. (2020). Ultraviolet radiation changes plant color. *BMC Plant Biology*, *20*(1). https://doi.org/10.1186/s12870-020-02471-8

Vernier. (2018, September 14). *What are the Best Light Sources for Photosynthesis?* https://www.vernier.com/2018/09/04/what-are-the-best-light-sources-for-photosynthesis/

Zegler, T.J.; Moore, M.M.; Fairweather, M.L.; Ireland, K.B.; Fulé, P.Z. (2012). Populus tremuloides mortality near the southwestern edge of its range. *Forest Ecological Management*, *282*(1), 196–207.

APPENDIX A

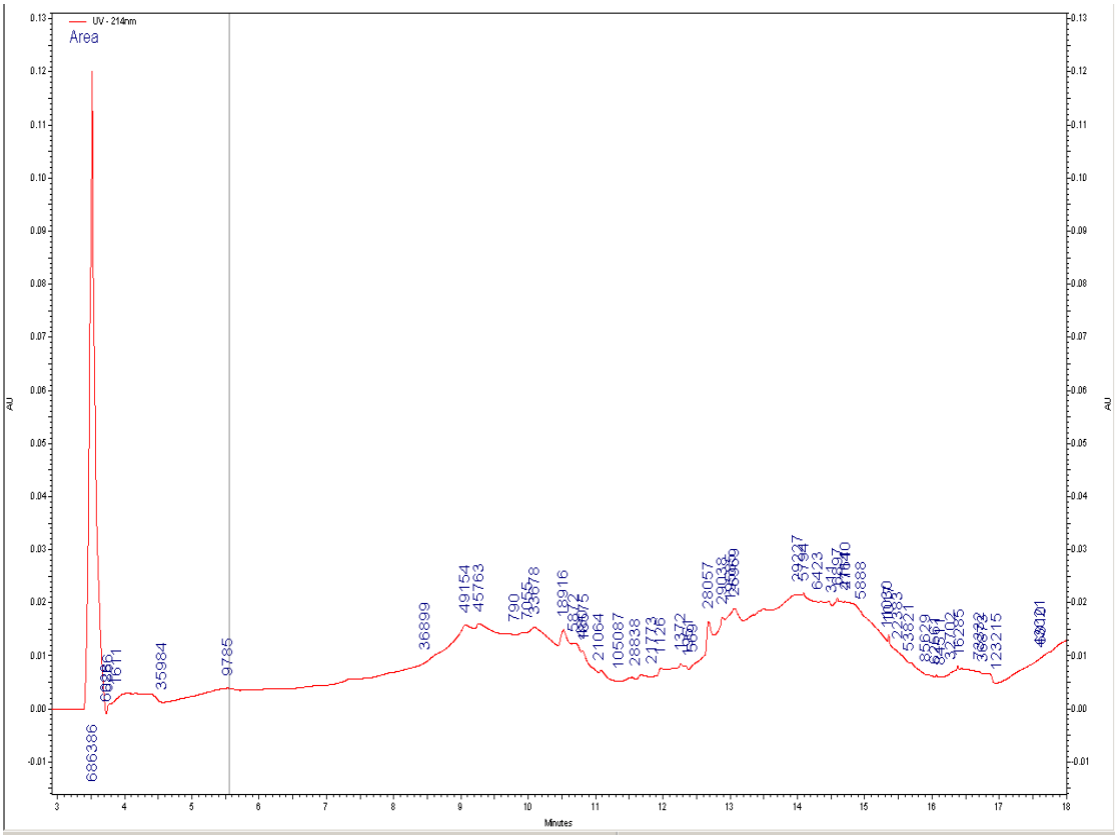

Figure A1. Electropherogram of $CDCl_3$ blank.

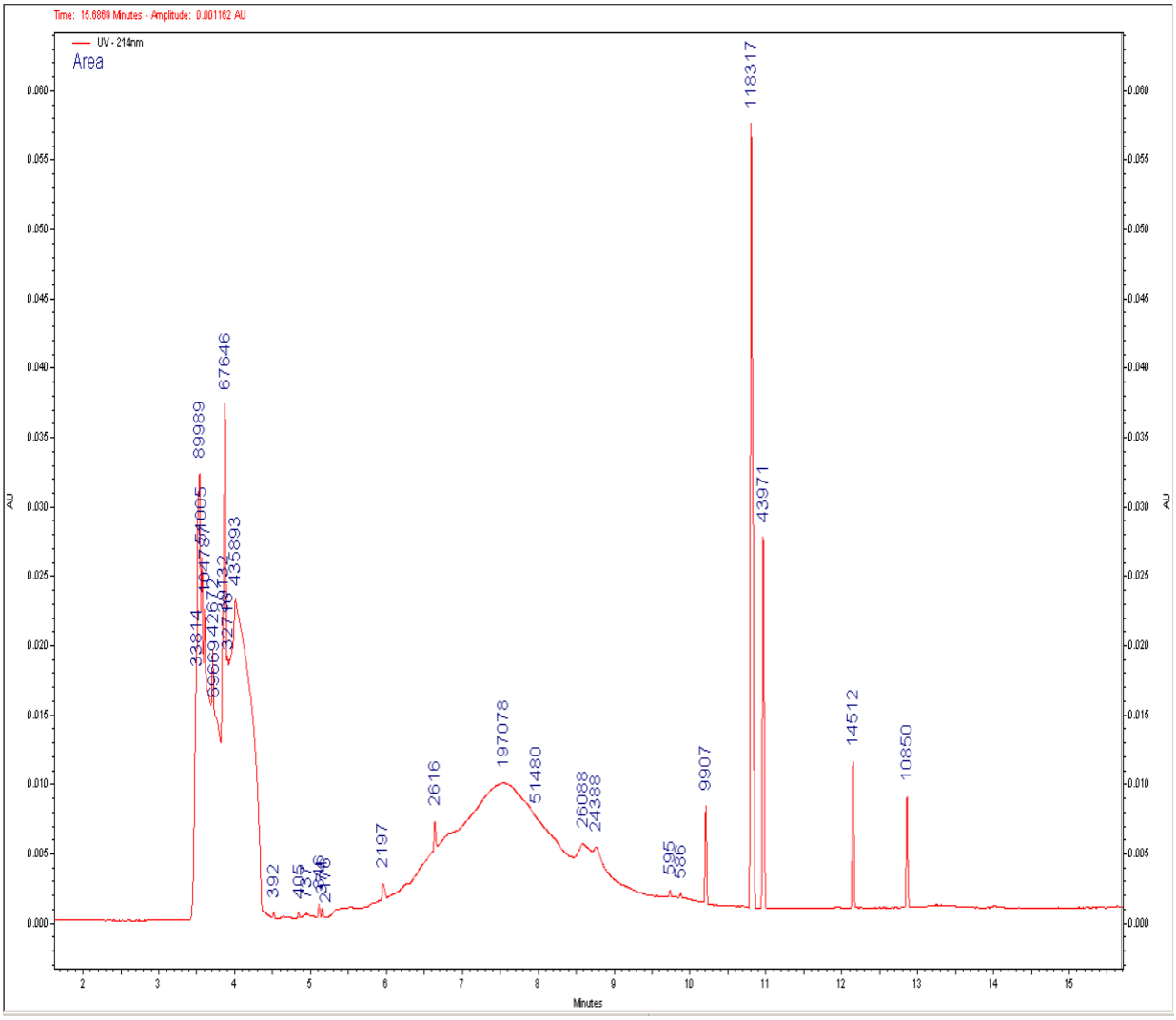

Figure A2. Electropherogram of hexane:ethyl acetate (4:1) blank (horizontal axis was cut off at 15 min since the remaining 5 min was baseline resolution).

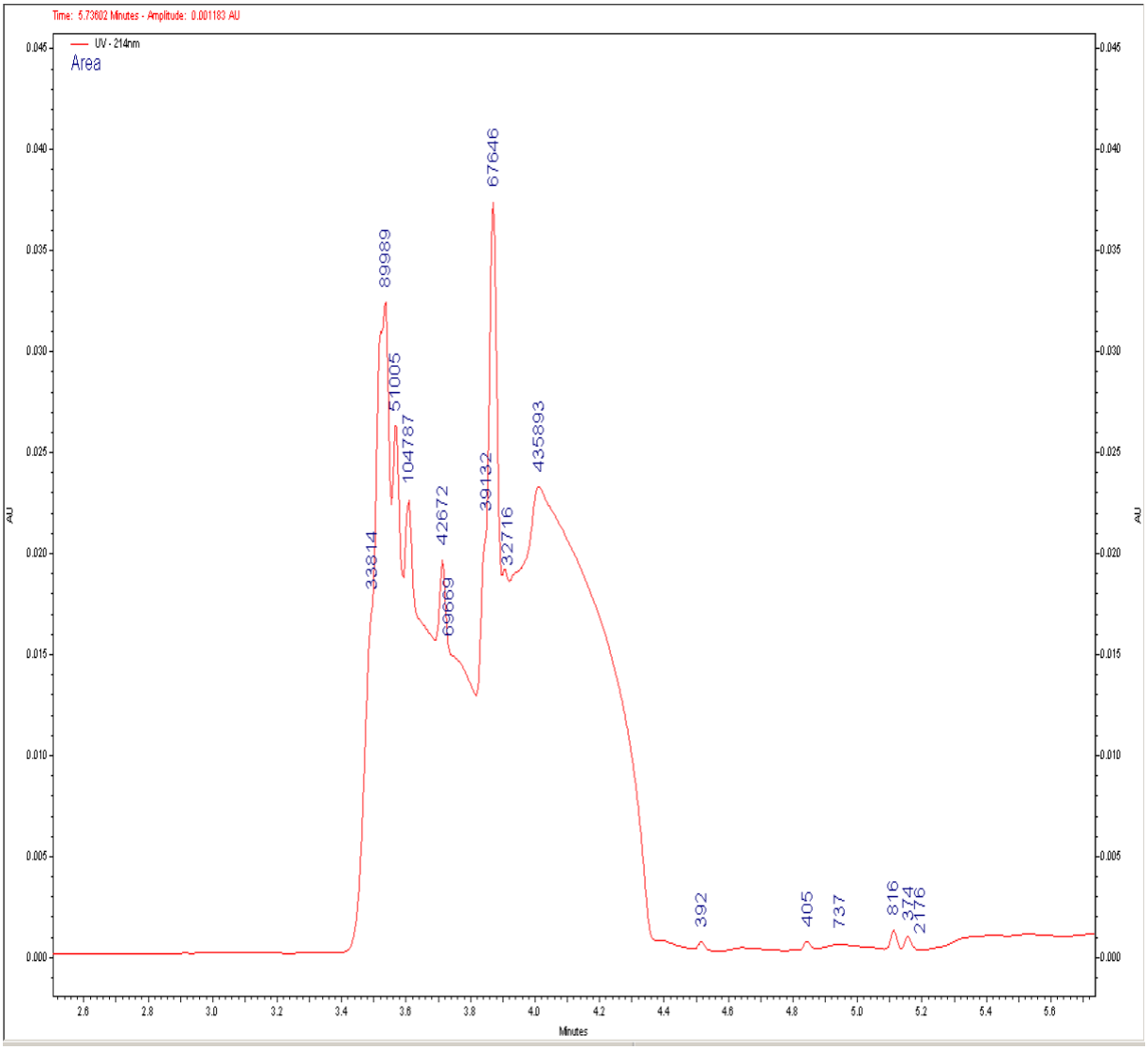

Figure A2(a). Zoomed electropherogram of hexane:ethyl acetate (4:1) blank.

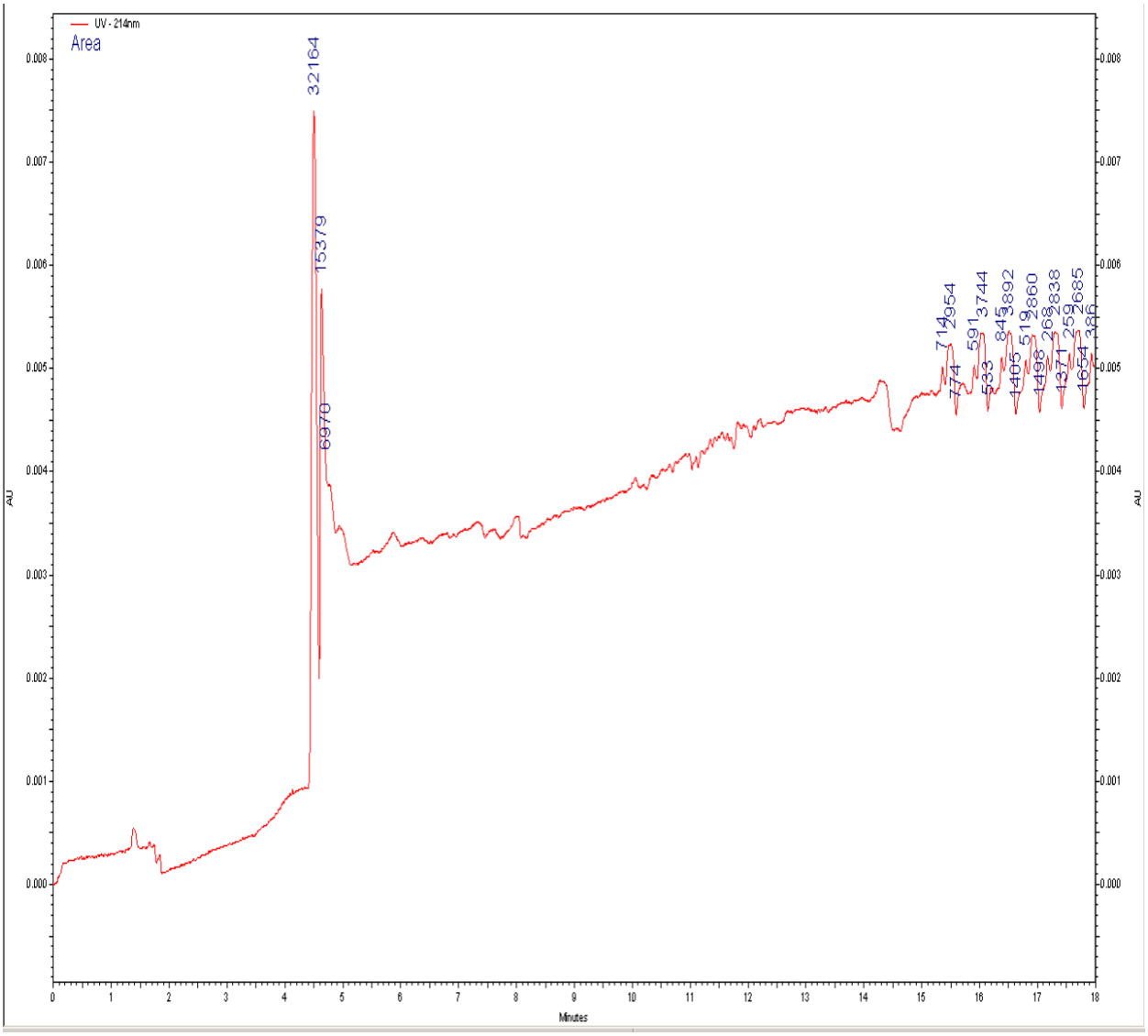

Figure A3. Electropherogram of 2 mL purified fraction in $CDCl_3$ and hexane:ethyl acetate (4:1).

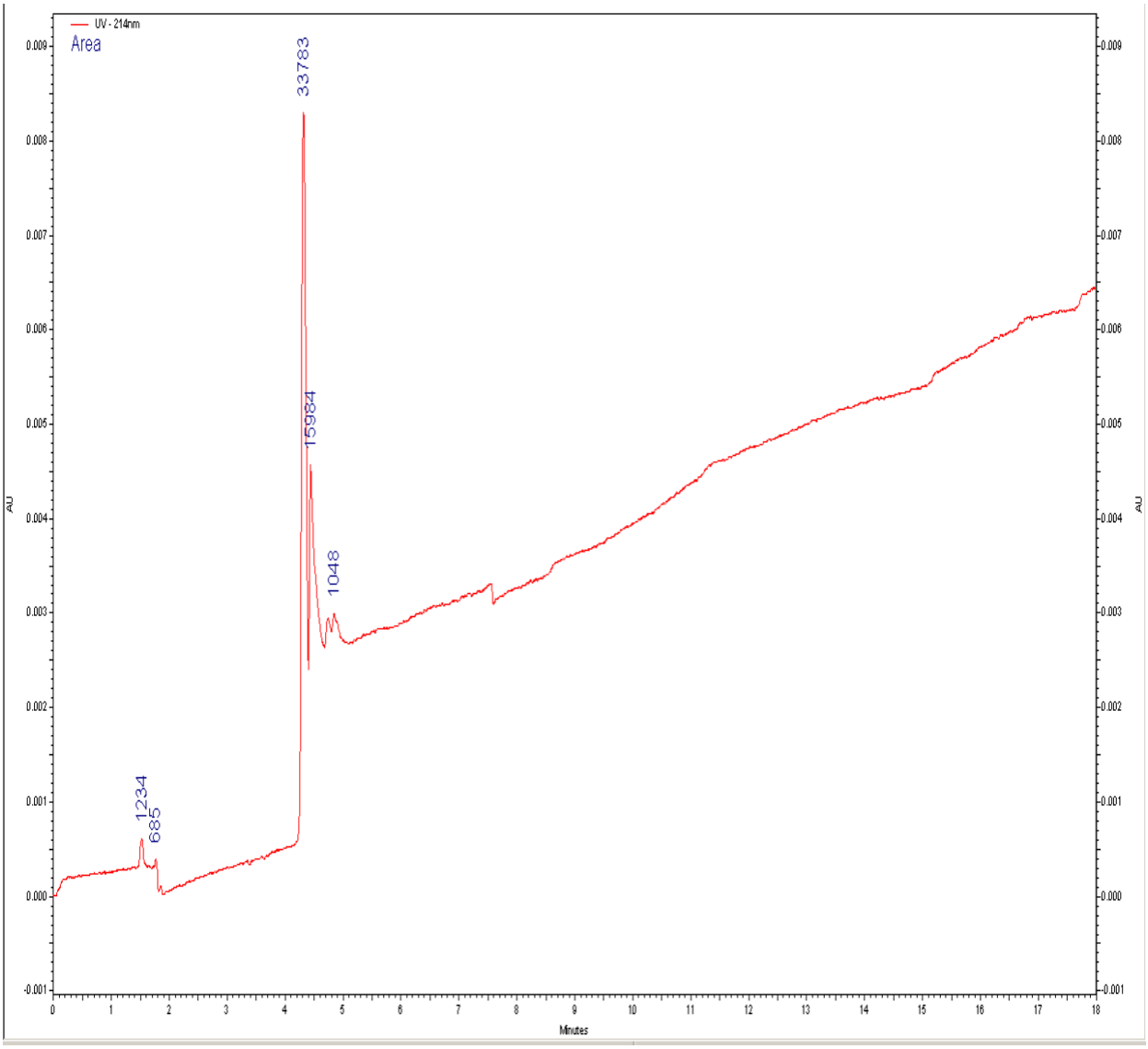

Figure A4. Electropherogram of 4 mL purified fraction in $CDCl_3$ and hexane:ethyl acetate (4:1).

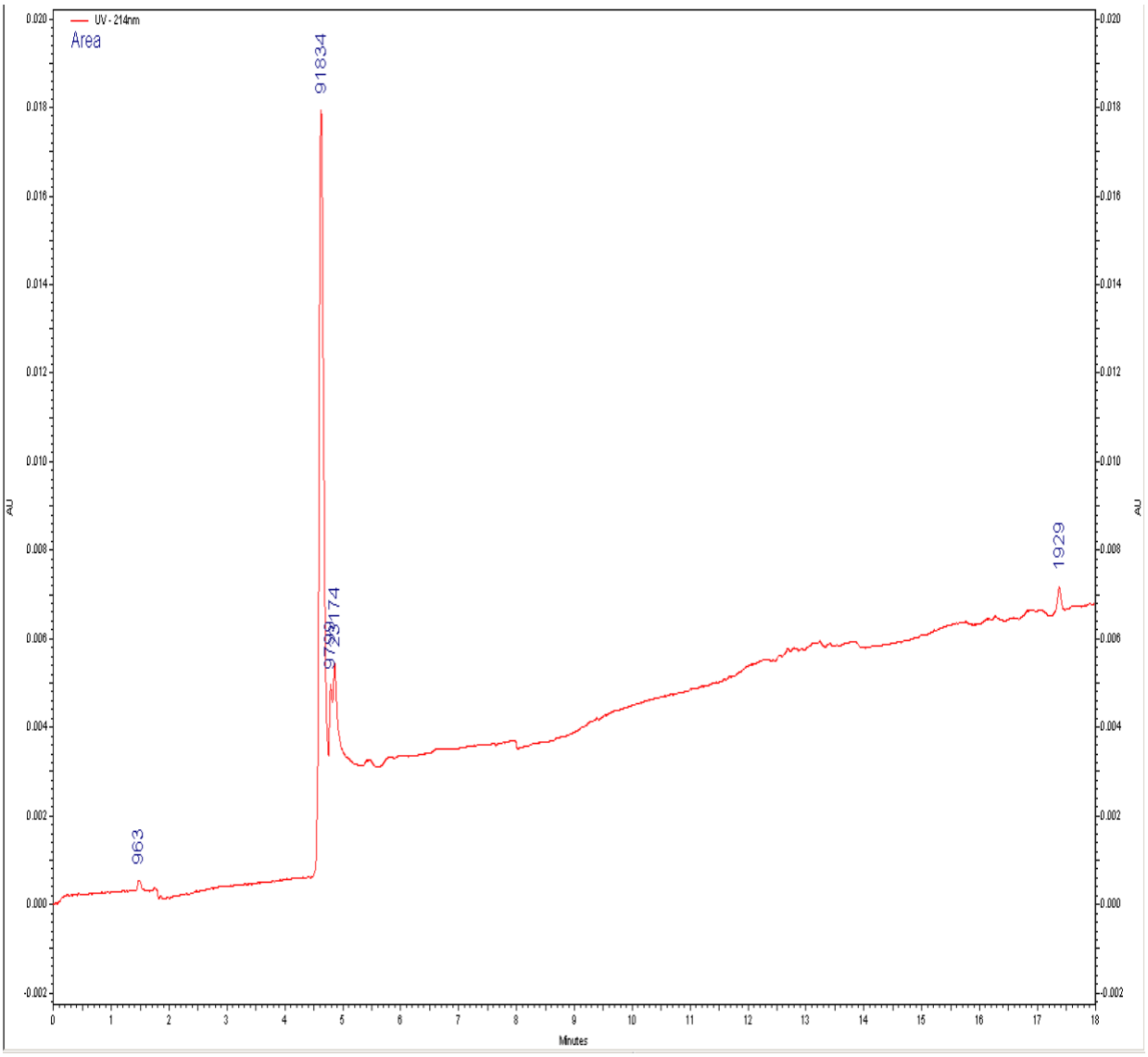

Figure A5. Electropherogram of 6 mL purified fraction in $CDCl_3$ and hexane:ethyl acetate (4:1).

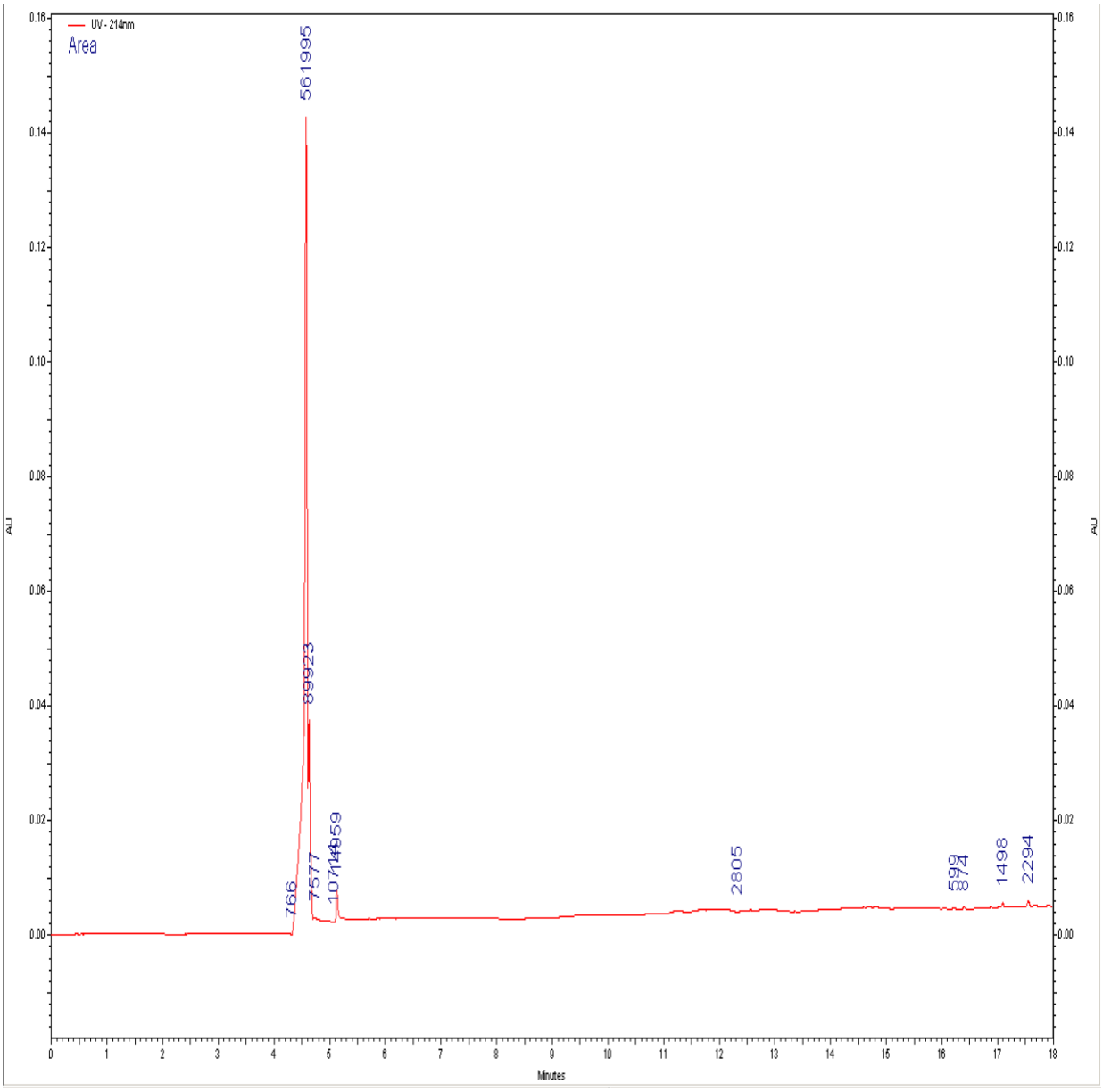

Figure A6. Electropherogram of 8 mL purified fraction in $CDCl_3$ and hexane:ethyl acetate (4:1).

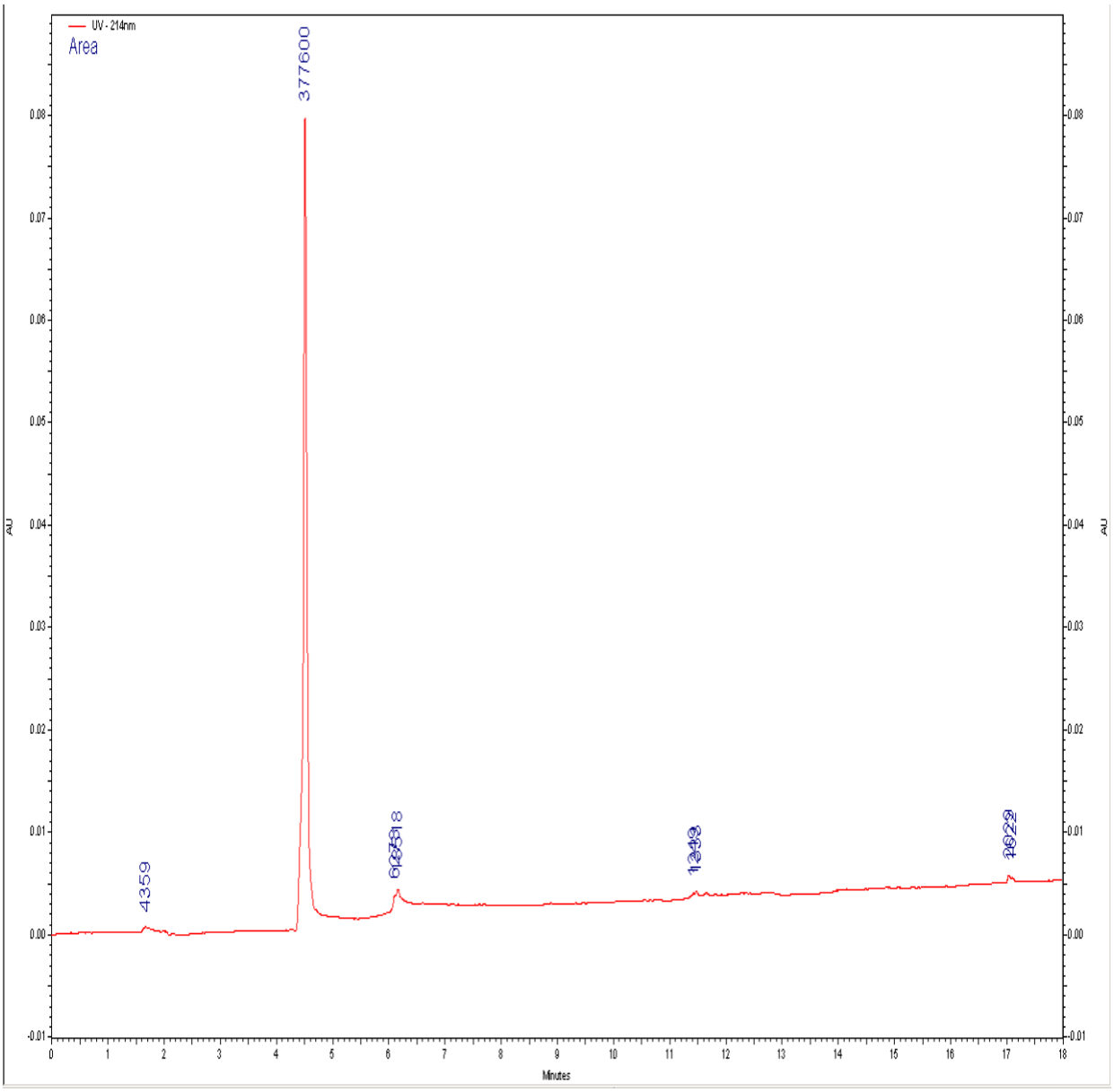

Figure A7. Electropherogram of 10 mL purified fraction in $CDCl_3$ and hexane:ethyl acetate (4:1).

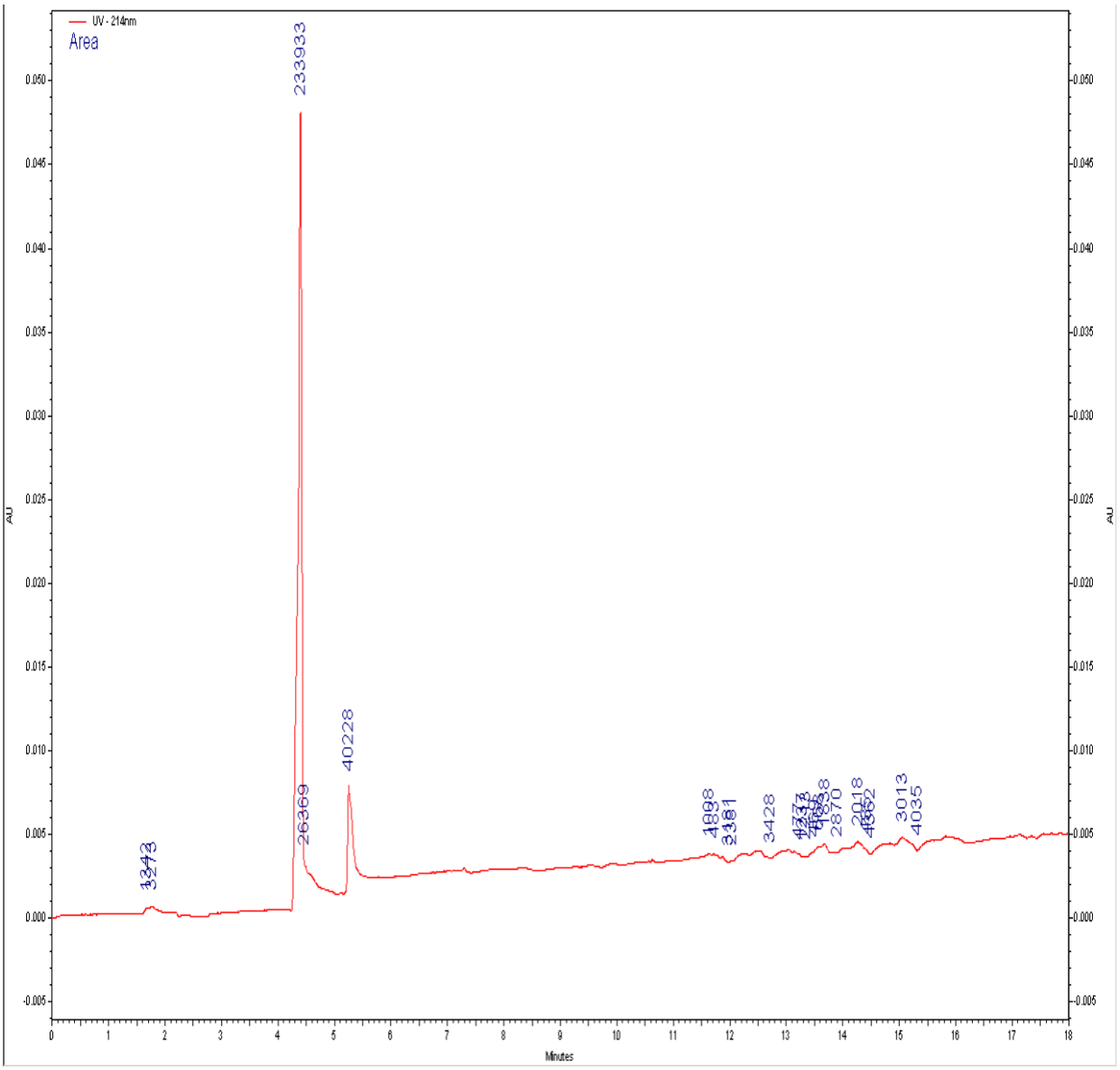

Figure A8. Electropherogram of 12 mL purified fraction in $CDCl_3$ and hexane:ethyl acetate (4:1).

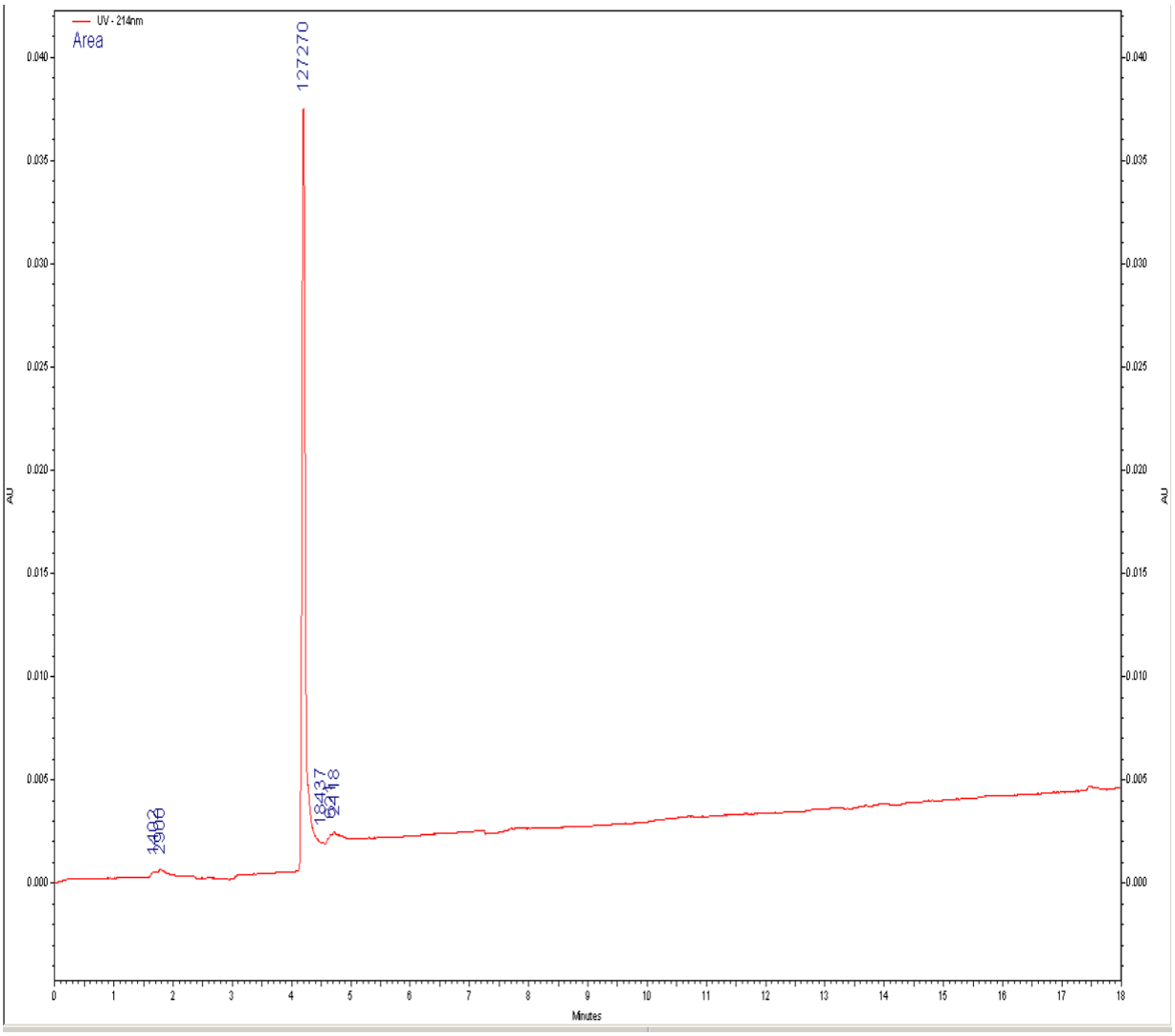

Figure A9. Electropherogram of 14 mL purified fraction in $CDCl_3$ and hexane:ethyl acetate (4:1).

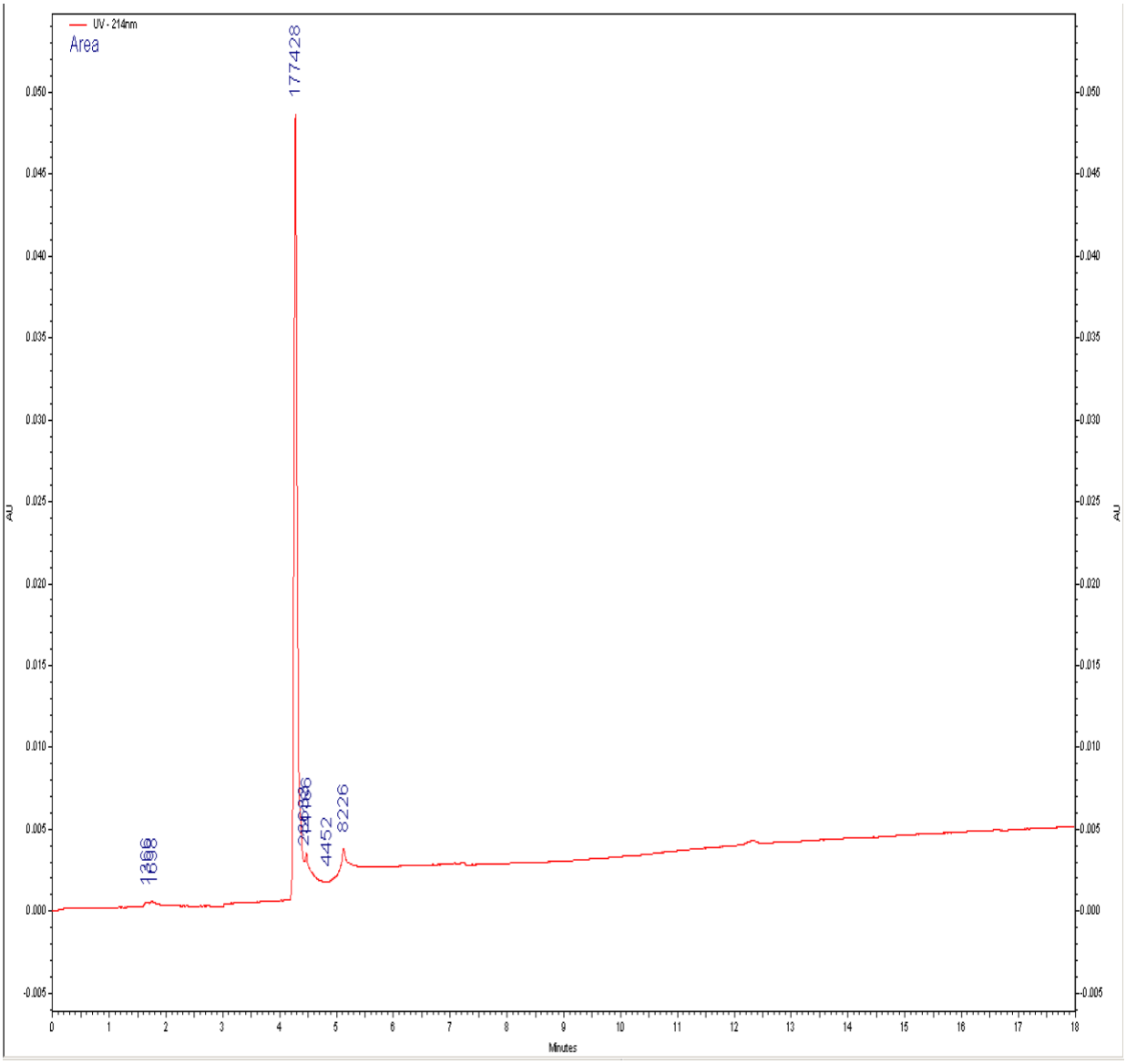

Figure A10. Electropherogram of 16 mL purified fraction in $CDCl_3$ and hexane:ethyl acetate (4:1).

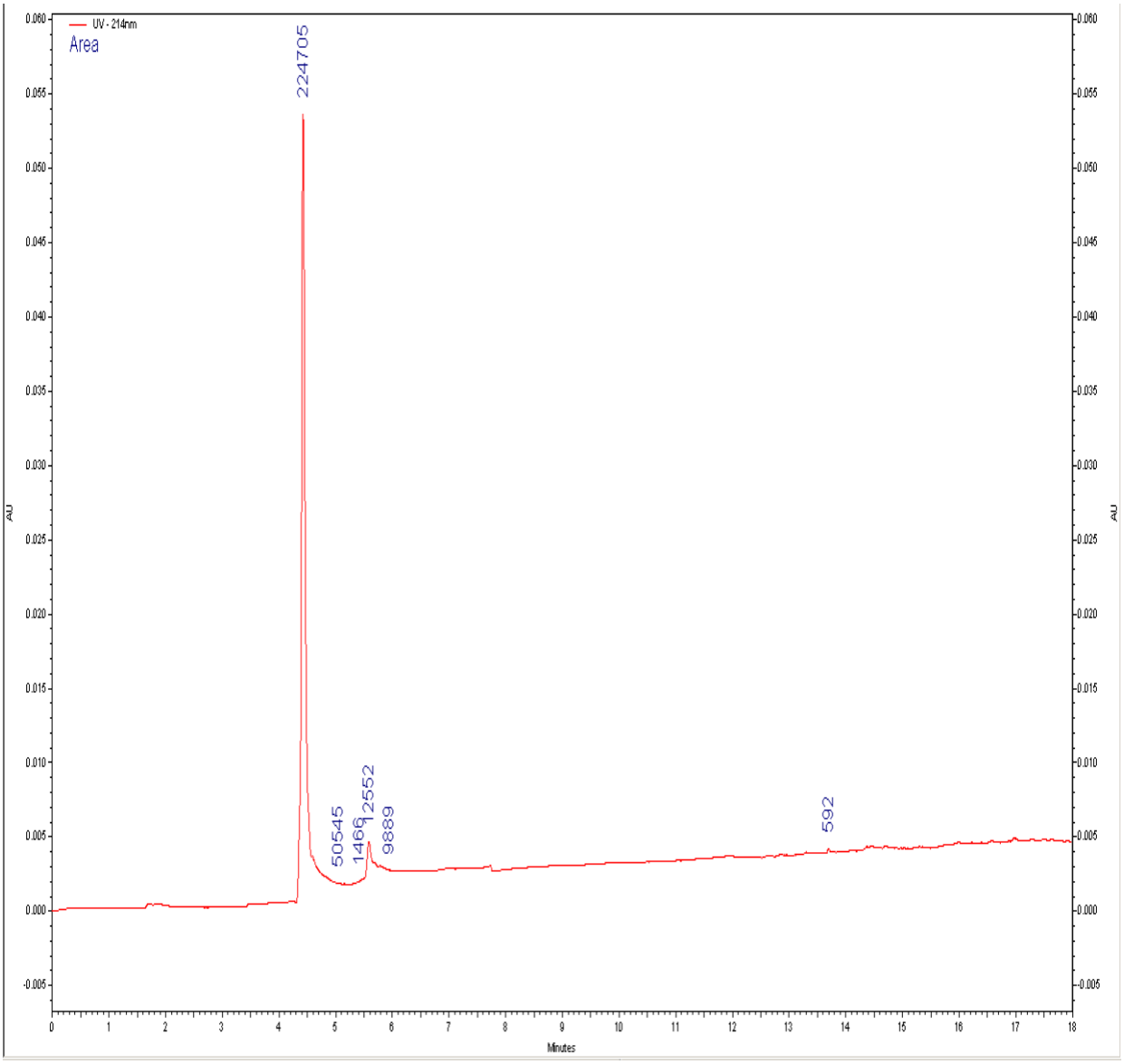

Figure A11. Electropherogram of 18 mL purified fraction in $CDCl_3$ and hexane:ethyl acetate (4:1).

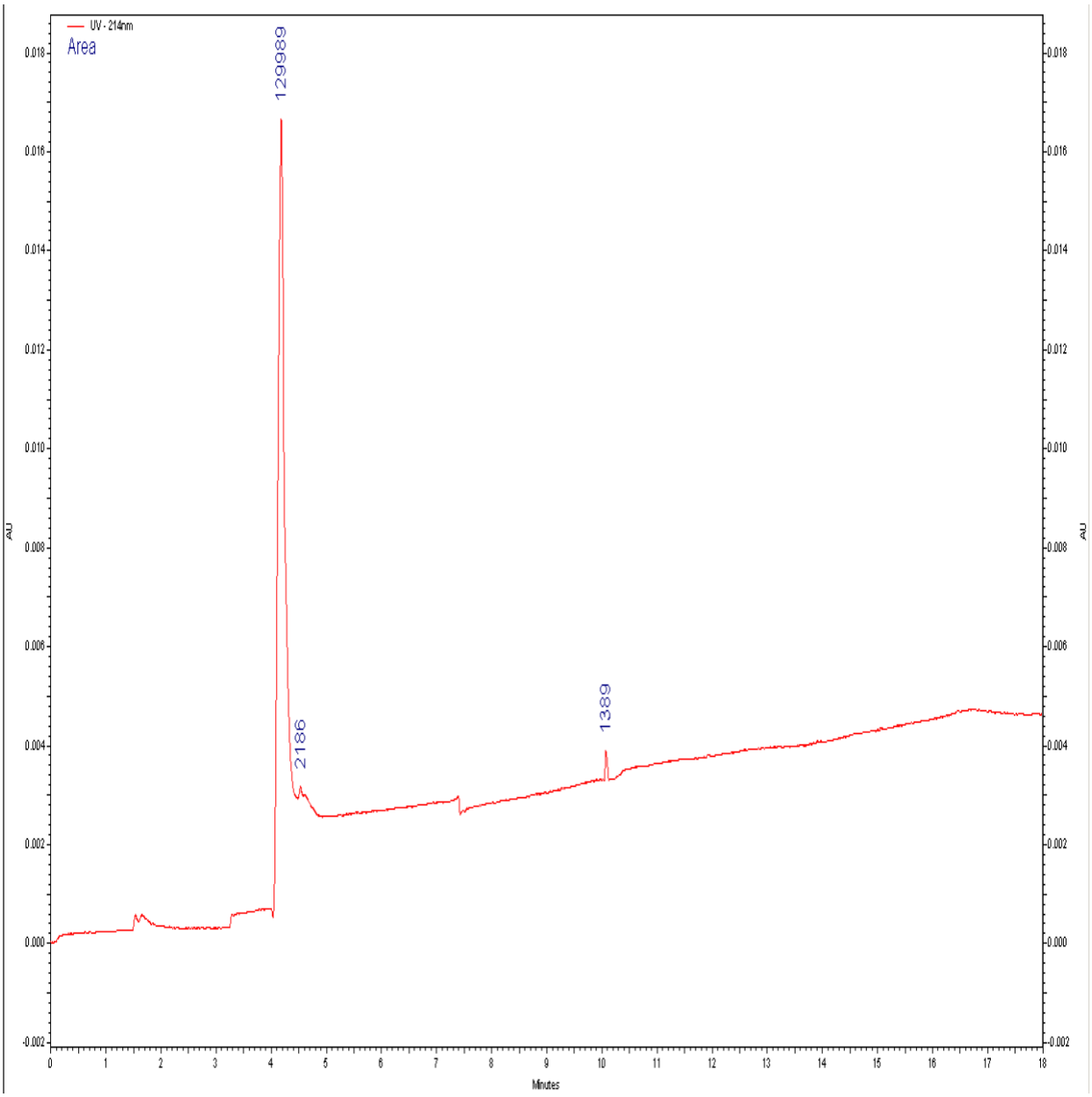

Figure A12. Electropherogram of 20 mL purified fraction in $CDCl_3$ and hexane:ethyl acetate (4:1).

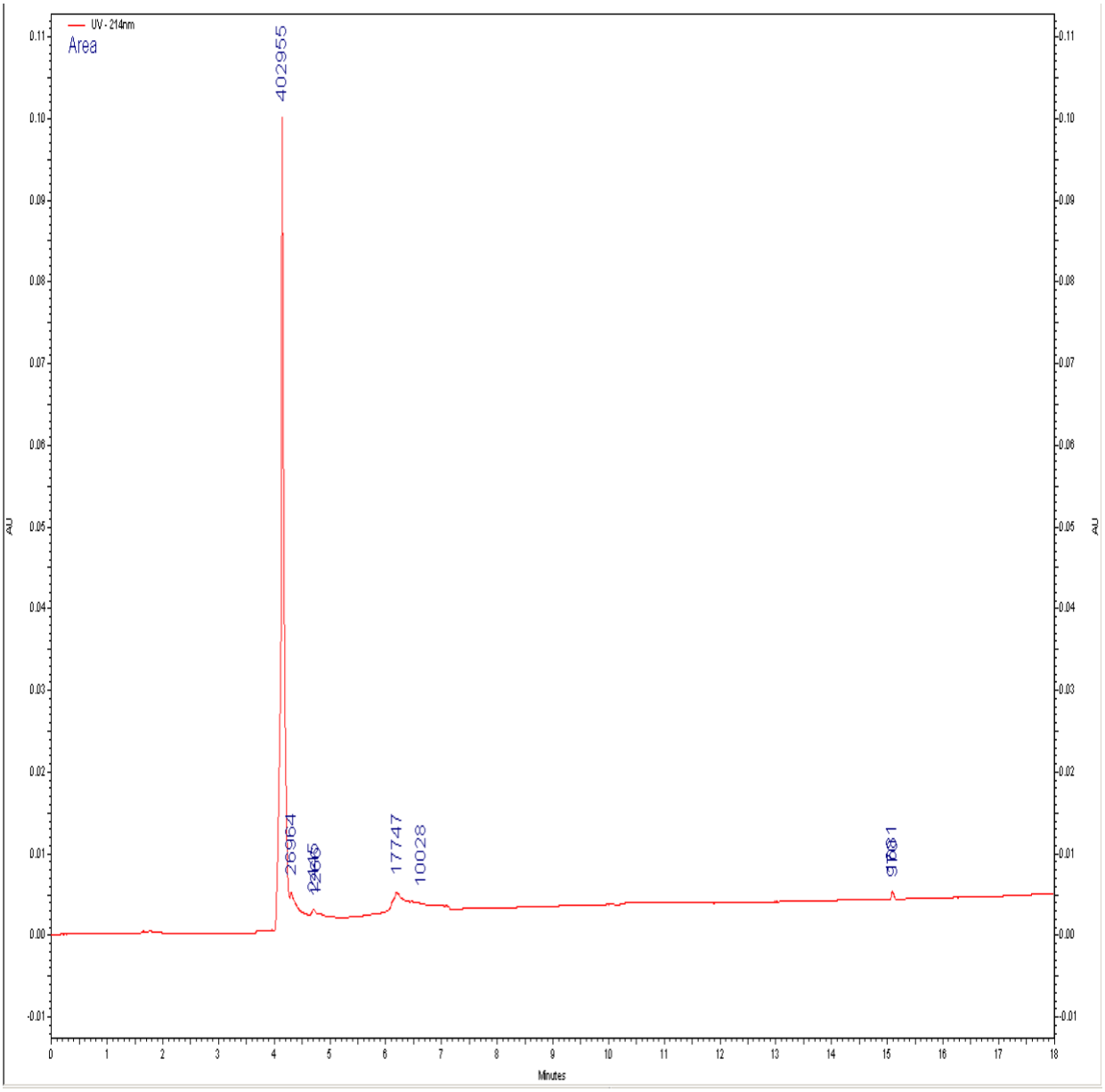

Figure A13. Electropherogram of 22 mL purified fraction in $CDCl_3$ and hexane:ethyl acetate (4:1).

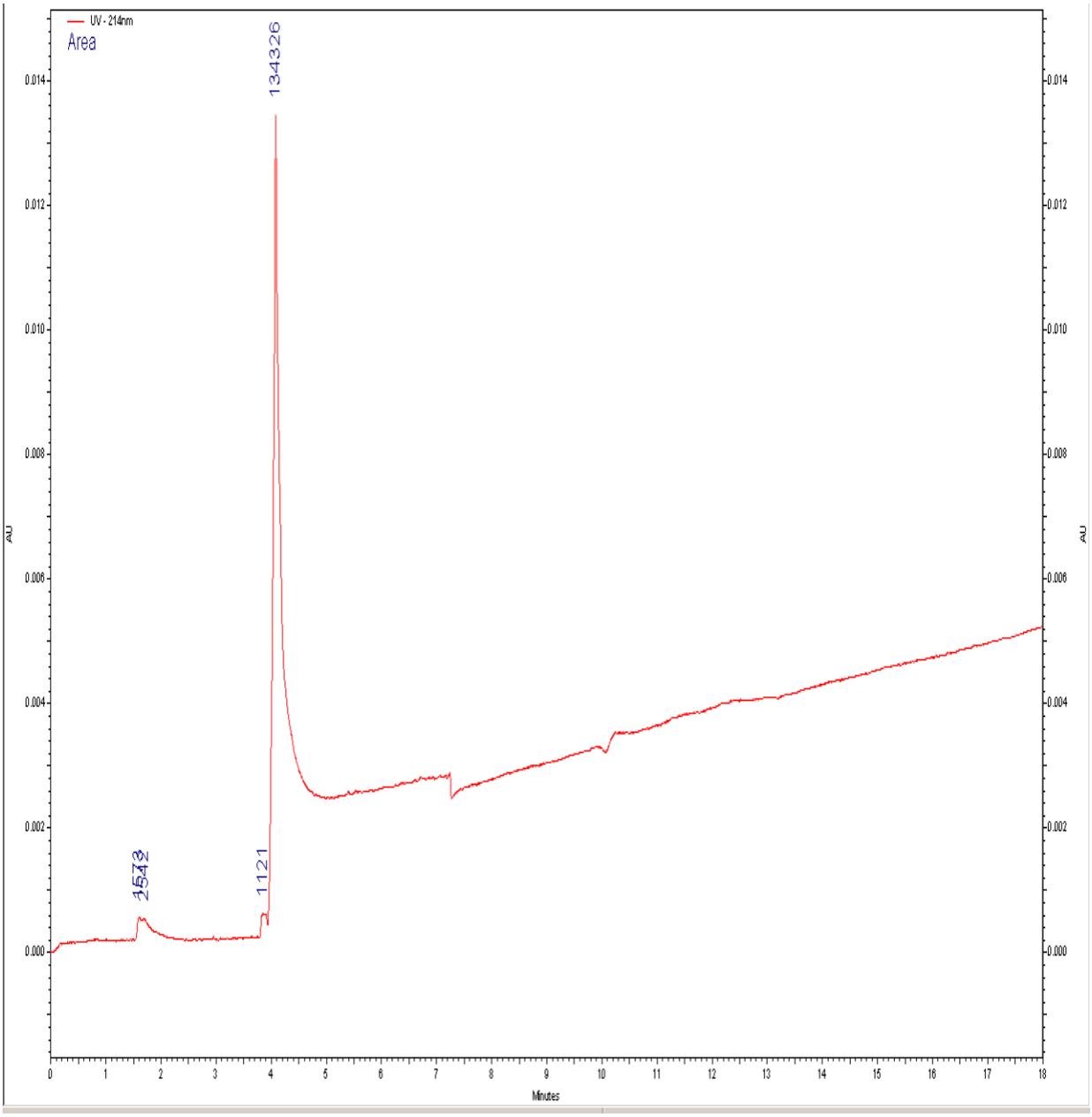

Figure A14. Electropherogram of 24 mL purified fraction in $CDCl_3$ and hexane:ethyl acetate (4:1).

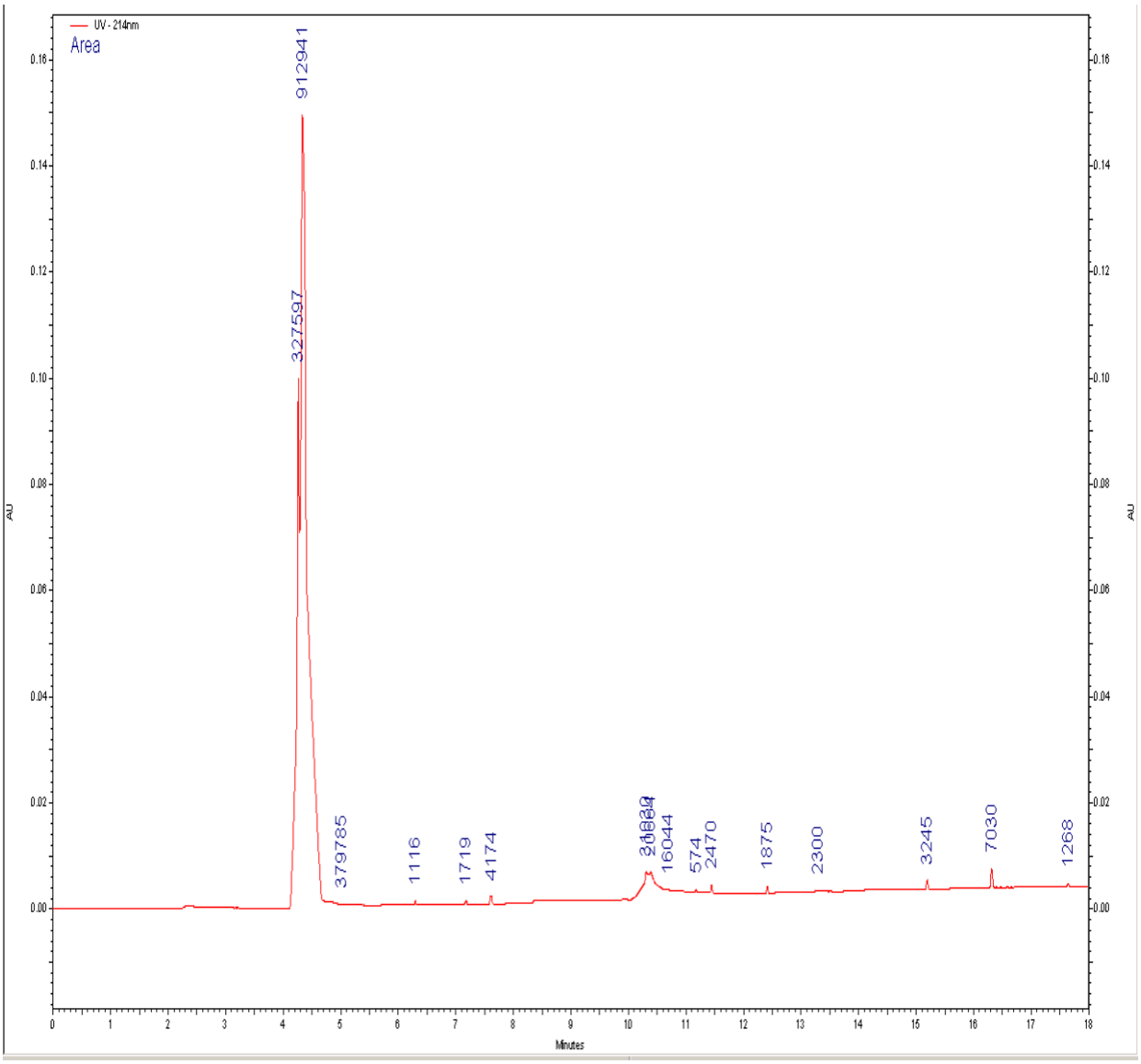

Figure A15. Electropherogram of 26 mL purified fraction in $CDCl_3$ and hexane:ethyl acetate (4:1).

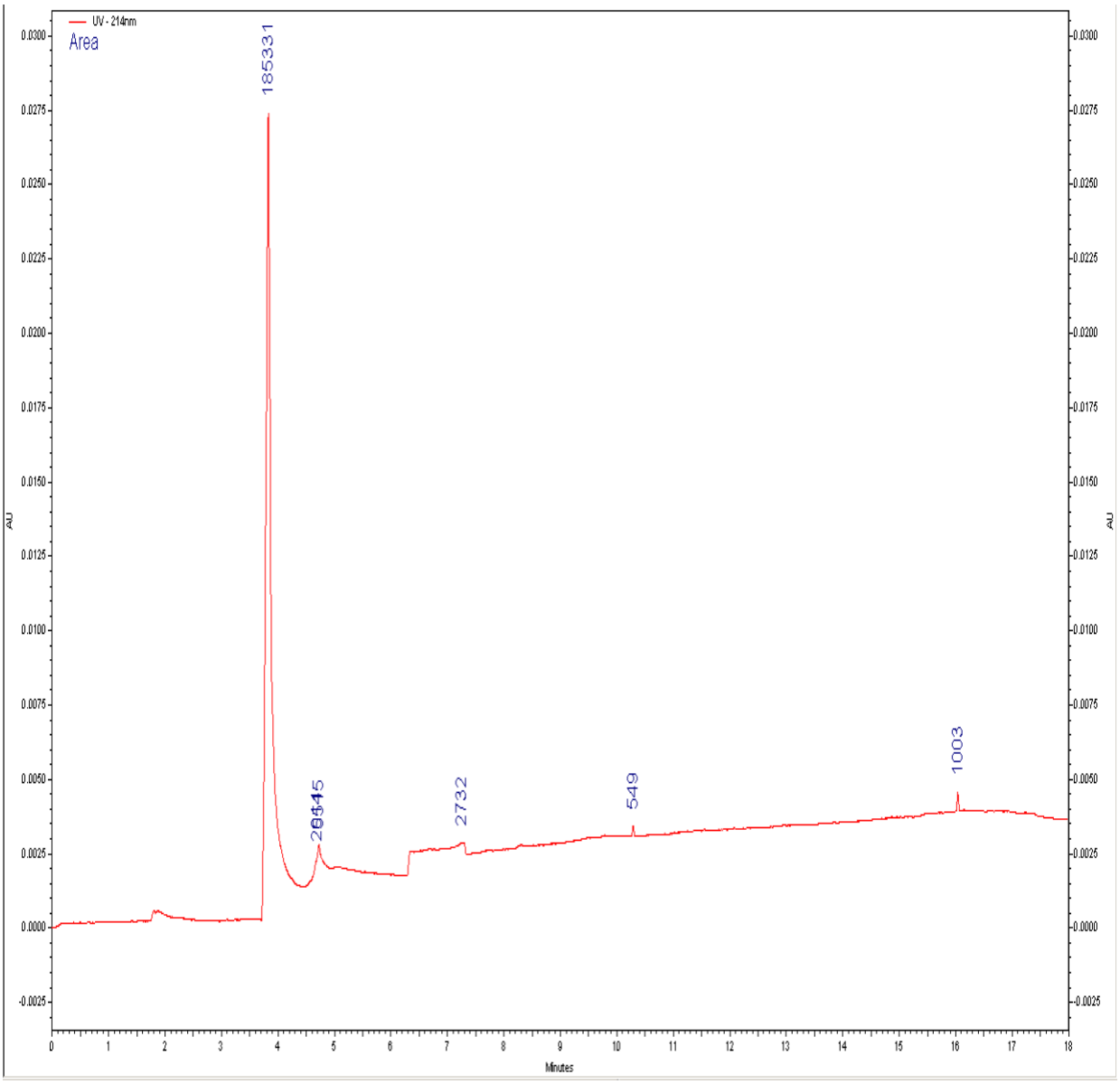

Figure A16. Electropherogram of 28 mL purified fraction in $CDCl_3$ and hexane:ethyl acetate (4:1).

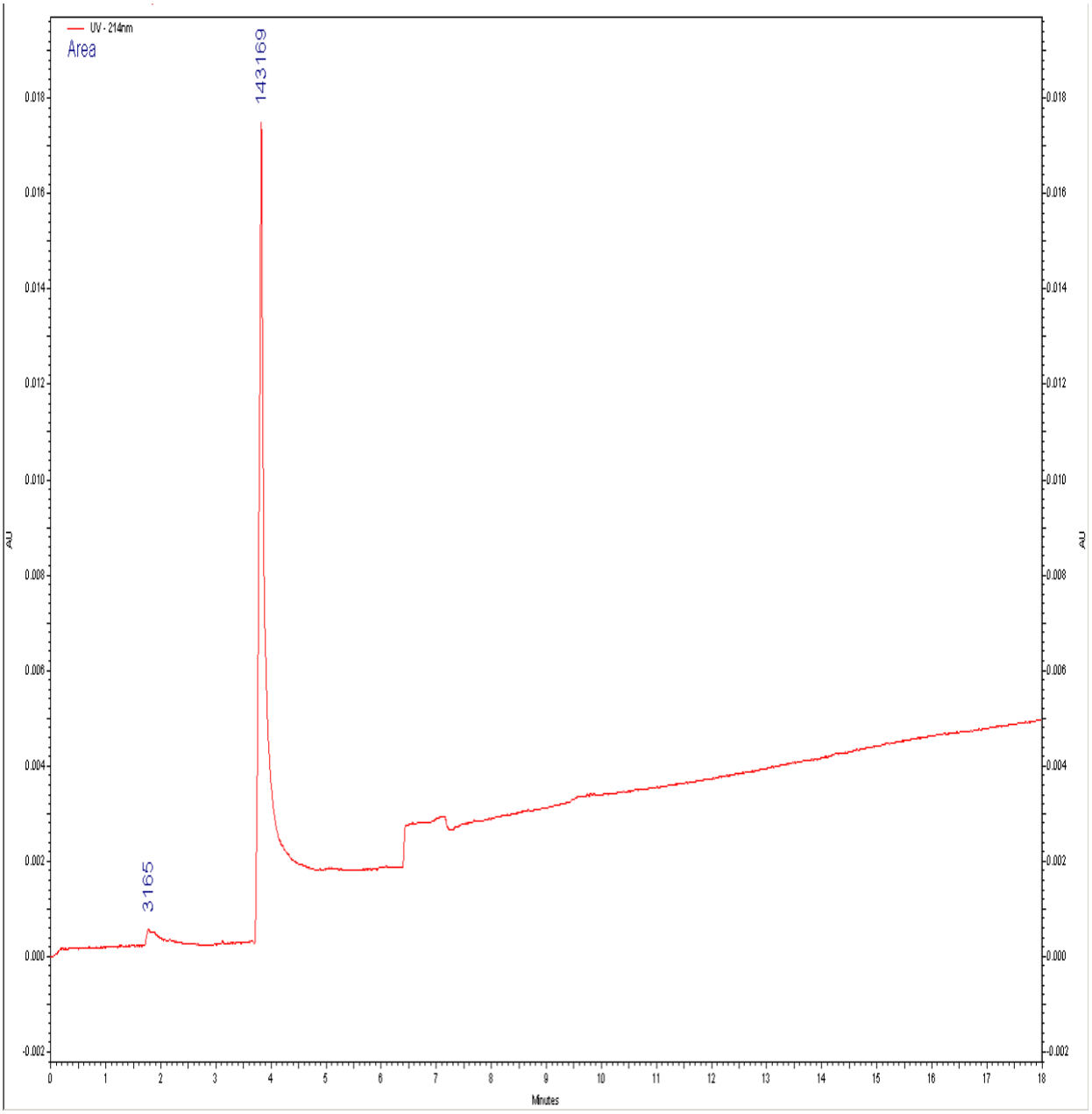

Figure A17. Electropherogram of 30 mL purified fraction in $CDCl_3$ and hexane:ethyl acetate (4:1).

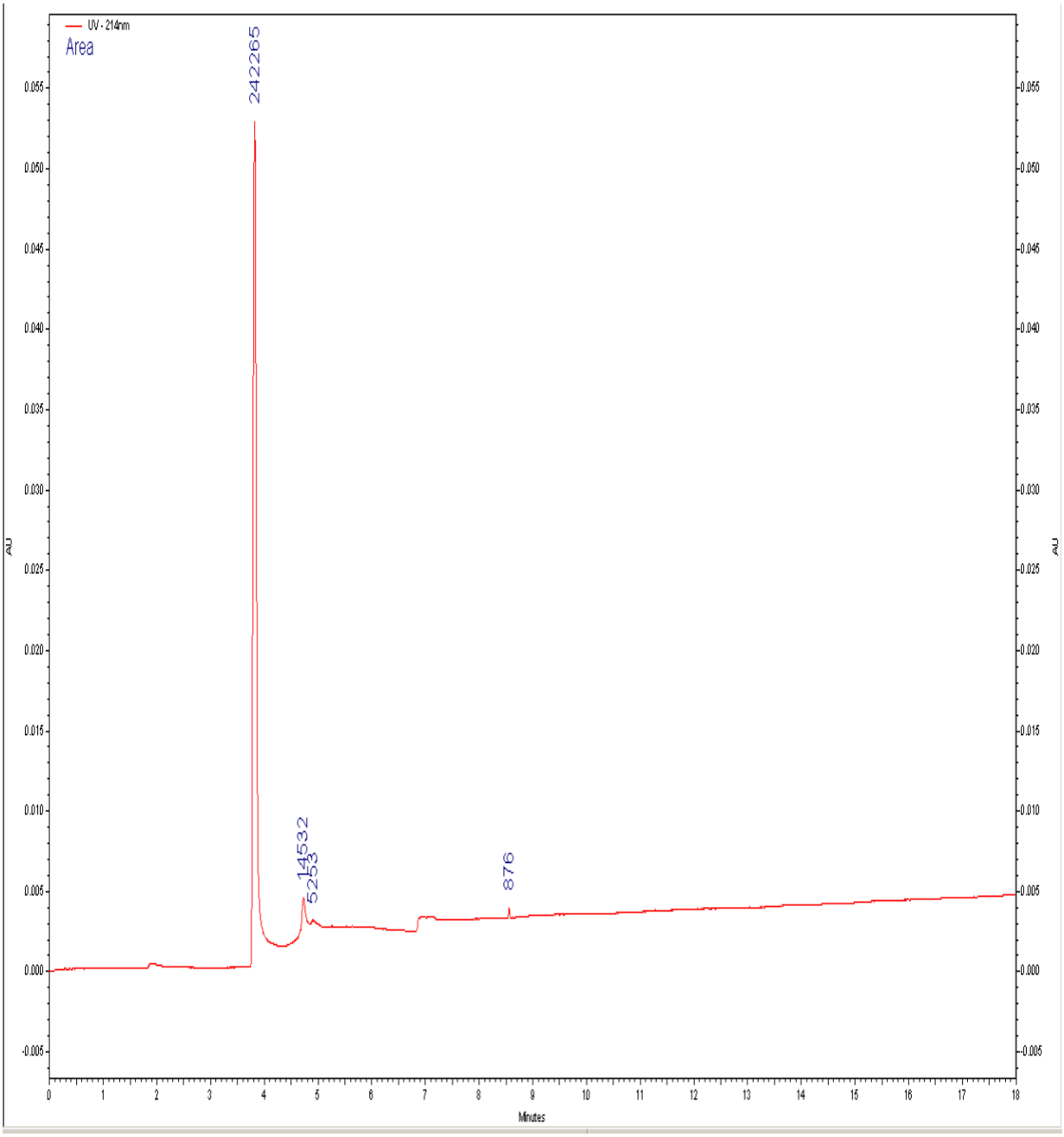

Figure A18. Electropherogram of 32 mL purified fraction in $CDCl_3$ and hexane:ethyl acetate (4:1).